STOCHASTIC ACCELERATION OF ELECTRONS AND PROTONS. I. ACCELERATION BY PARALLEL-PROPAGATING WAVES

Vahé Petrosian[1] and Siming Liu

Center for Space Science and Astrophysics, Department of Physics, Stanford University, Stanford, CA 94305;
vahe@astronomy.stanford.edu, liusm@stanford.edu

ABSTRACT

Stochastic acceleration of electrons and protons by waves propagating parallel to the large-scale magnetic fields of magnetized plasmas is studied with emphasis on the feasibility of accelerating particles from a thermal background to relativistic energies and with the aim of determining the relative acceleration of the two species in one source. In general, the stochastic acceleration by these waves results in two distinct components in the particle distributions, a quasi-thermal and a hard nonthermal, with the nonthermal one being more prominent in hotter plasmas and/or with higher level turbulence. This can explain many of the observed features of solar flares. Regarding the proton-to-electron ratio, we find that in a pure hydrogen plasma the dominance of the wave-proton interaction by the resonant Alfvén mode reduces the acceleration rate of protons in the intermediate energy range significantly, while the electron-cyclotron and Whistler waves are very efficient in accelerating electrons from a few keV to MeV energies. The presence of such an acceleration barrier prohibits the proton acceleration under solar flare conditions. This difficulty is alleviated when we include the effects of ^{4}He in the dispersion relation and the damping of the turbulent waves by the thermal background plasma. The additional ^{4}He cyclotron branch of the turbulent plasma waves suppresses the proton acceleration barrier significantly, and the steep turbulence spectrum in the dissipation range makes the nonthermal component have a near power-law shape. The relative acceleration of protons and electrons is very sensitive to a plasma parameter $\alpha = \omega_{pe}/\Omega_e$, where ω_{pe} and Ω_e are the electron plasma frequency and gyrofrequency, respectively. Protons are preferentially accelerated in weakly magnetized plasmas (large α). The formalism developed here is applicable to the acceleration of other ion species and to other astrophysical systems.

Subject headings: acceleration of particles — MHD — plasmas — Sun: flares — turbulence

On-line material: color figures

1. INTRODUCTION

One of the important questions in acceleration of cosmic particles is the fractions of energy that go into acceleration of electrons and protons (and other ions). In this paper we investigate this question for acceleration by plasma wave turbulence, a second-order Fermi acceleration process, which we call stochastic acceleration (SA). The theory of SA has received little attention in high-energy astrophysics except in solar flares where it has achieved significant successes during the past few years. The turbulence or plasma waves required for this model are presumably generated during the magnetic reconnection that energizes the flares. The first application of SA was to the acceleration of protons and other ions to explain the observed nuclear gamma-ray lines from solar flares (see, e.g., Ramaty 1979; Miller & Roberts 1995). Combining with the nuclear reaction rates (Ramaty et al. 1975, 1979; see also Kozlovsky et al. 2002) and a magnetic loop model, Hua & Lingenfelter (1987a, 1987b) and Hua et al. (1989) showed that the SA model can provide natural explanations for the many observed features in the 1–7 MeV range. Later this model was also investigated in the acceleration of electrons in several studies (Miller & Ramaty 1987; Bech et al. 1990; Miller et al. 1996; Park & Petrosian 1995, 1996), and the first quantitative comparison of predictions of this model with the observed

hard X-ray (10–200 keV) spectra in some solar flares was carried out by Hamilton & Petrosian (1992). With a more detailed modeling, Park et al. (1997) showed that the SA of electrons by some generic turbulent plasma waves can reproduce the many spectral breaks observed over a broad energy range, from tens of keV to ∼100 MeV, in the so-called electron-dominated flares via the bremsstrahlung process (Rieger et al. 1998; Petrosian et al. 1994).

The strongest evidence supporting the SA model comes from the *Yohkoh* discovery of impulsive hard X-ray emission from the top of a flaring loop, in addition to previously known emission from loop footpoints (FPs; Masuda et al. 1994; Masuda 1994). The presence of the loop-top (LT) emission requires temporary trapping of the accelerated electrons at the top of the loop where the reconnection is taking place. The turbulence required for SA will naturally accomplish this by repeated scatterings of the particles (Petrosian & Donaghy 1999). More importantly, an analysis of a larger sample of *Yohkoh* flares (Petrosian et al. 2002) has shown that the LT emission is a common property of all flares, and a preliminary investigation of *RHESSI* data appears to confirm this picture (Liu et al. 2003). Finally, a third and equally important piece of evidence in support of the SA model comes from the spectra and relative abundances of the flare-accelerated protons and other ions observed at 1 AU from the Sun (Mazur et al. 1992; Reames et al. 1994; Miller 2003). These several independent lines of argument have established the SA as the leading model for solar flares. This may be also true in many

[1] Department of Applied Physics, Stanford University, Stanford, CA 94305.

other astrophysical nonthermal sources. Thus, a more detailed investigation of the SA model and its comparison with observations are now fully warranted.

In particular, the SAs of electrons on the one hand and protons and other ions on the other are investigated separately; a unified treatment and comparison with the total nonthermal radiative signatures of all species have not been carried out yet. The purpose of this investigation is to obtain the relative acceleration of electrons and protons from the thermal backgrounds of solar flare plasmas with the same spectrum of turbulence. We present some general results of the model and qualitative comparisons with observations. More detailed comparisons with observations and the acceleration of other ions, such as the anomalous overabundance of the flare-accelerated ^{3}He, will be addressed in subsequent papers. Specifically, we will address the energy partition between the flare-accelerated electrons and protons. Observationally, in some flares, or during the earlier impulsive phase of most flares, there is little evidence for gamma-ray lines and therefore proton acceleration. These are called electron-dominated cases. In the majority of solar flares the energy partition favors electrons, but there are a significant fraction of flares where more energy resides in protons than in electrons in their respective observed energy bands. The ratio of energy of the observed electrons (with greater than 20 keV range) to that of protons (with greater than 1 MeV range) in solar flares varies approximately from 0.03 to 100 (see, e.g., a compilation by Miller et al. 1997). In what follows, we use solar flare plasma conditions, but the formalism described here is applicable to other astrophysical sources.

In § 2 we describe the general theory of SA and argue that in most cases the Fokker-Planck (F-P) equation can be reduced to the diffusion-convection equation with the corresponding coefficients given by pitch-angle–averaged combinations of the F-P coefficients. In § 3 we study the resonant interactions of electrons and protons with parallel-propagating waves in a pure hydrogen plasma and calculate the resultant F-P coefficients and acceleration parameters for interactions with a power-law turbulence spectrum of the wavenumber. The new and surprising result here is that the proton acceleration is suppressed by a barrier in its acceleration rate in the intermediate energy range. This is what is required by observations of electron-dominated cases, but as shown in this paper, this barrier is too strong and makes the acceleration of protons unacceptably inefficient relative to the electron acceleration, except for in very weakly magnetized plasmas. In § 4 we point out that this difficulty can be alleviated by a more complete description of the dispersion relation that includes the effects of helium ions and by an inclusion of the effects of the thermal damping of the turbulence at high wavenumbers. The presence of an appropriate amount of fully ionized helium introduces an extra wave branch that lowers the barrier, and the thermal damping steepens the turbulence spectrum toward high wavenumbers, making the acceleration of electrons and protons more in agreement with observations. The results presented here are summarized in § 5, and their applications to solar flare observations are discussed qualitatively. Some useful approximate analytical expressions for the interaction rates are presented in Appendices A, B, C, and D.

2. GENERAL THEORY OF STOCHASTIC ACCELERATION

In this section we present the general theory of SA and show that in most astrophysical situations the diffusion-convection equation is adequate to address the particle acceleration processes.

2.1. Fokker-Planck Equation

The study of SA in a magnetized plasma starts from the collisionless Boltzmann-Vlasov equation and the Lorentz force (Schlickeiser 1989). In the quasi-linear approximation, it can be treated by the F-P equation (e.g., Kennel & Engelmann 1966):

$$\frac{\partial f}{\partial t} + v \frac{\partial f}{\partial s} = \frac{1}{p^2} \frac{\partial}{\partial p} p^2 \left(D_{pp} \frac{\partial f}{\partial p} + D_{p\mu} \frac{\partial f}{\partial \mu} \right)$$
$$+ \frac{\partial}{\partial \mu} \left(D_{\mu\mu} \frac{\partial f}{\partial \mu} + D_{\mu p} \frac{\partial f}{\partial p} \right) - \frac{1}{p^2} \frac{\partial}{\partial p} \left(p^2 \dot{p}_L f \right) + S,$$

(1)

where the wave-particle interaction is parameterized by the F-P coefficients $D_{ij}[i, j \in (\mu, p)]$. Here $f(t, s, p, \mu)$ is the gyrophase-averaged particle distribution and s, v, μ, and p are the spatial coordinate along the field lines, the velocity, the pitch-angle cosine, and the momentum of the particle, respectively. The energy-loss (minus systematic energy gains, if any) processes are accounted for by $\dot{p}_L$, and S is the source function.

For weak turbulence ($\delta B \ll B$), as is the case for solar flares, the F-P coefficients can be evaluated by assuming that the particles and waves are coupled via a resonant process. The acceleration of particles at a given energy is then dominated by interactions with certain specific wave modes, e.g., the Alfvén or Whistler waves. For a study of acceleration in a narrow energy band it is usually sufficient to consider waves in a narrow frequency range (Miller & Ramaty 1987). In order to address the energy partition between electrons and ions, however, one has to calculate the particle acceleration over the whole energy range. For example, the Alfvén waves can efficiently accelerate ions but not nonrelativistic electrons. Models with pure Alfvénic turbulence are not adequate to address the energy partition of accelerated particles in solar flares and many other astrophysical plasmas, especially for the acceleration of particles from a thermal background. For the acceleration of such low-energy particles interactions with turbulent plasma waves extending over a broad range of wavenumbers (and frequencies) must be considered. We consider here interactions with a broad spectrum of plasma waves propagating along a static background magnetic field. The interactions of parallel-propagating waves with electrons are described fully by Dung & Petrosian (1994, hereafter DP94) and Pryadko & Petrosian (1997, hereafter PP97) (see also Steinacker & Miller 1992). We use their formalism and evaluate the relative rates of interaction and acceleration of electrons and protons in cold but fully ionized plasmas.

2.2. Dispersion Relation and Resonance Condition

Waves propagating parallel or antiparallel to the large-scale magnetic field in a uniform plasma have two normal modes that are polarized circularly (Sturrock 1994). Because their electric fields are perpendicular to their corresponding wavevectors, the waves are also referred to as transverse waves. The dispersion relation for these waves in a cold plasma is (see DP94)

$$(kc)^2 = \omega^2 \left[1 - \sum_i \frac{\omega_{pi}^2}{\omega(\omega + \Omega_i)} \right],$$

(2)

where $\omega_{pi} = (4\pi n_i q_i^2/m_i)^{1/2}$ and $\Omega_i = (q_i B_0)/(m_i c)$ are, respectively, the plasma frequencies and the nonrelativistic gyrofrequencies of the background particles (with charges q_i, masses m_i, and number densities n_i). The term B_0 stands for the large-scale magnetic field, c is the speed of light, and ω and k are the wave frequency and wavenumber, respectively.

One of the important parameters characterizing a magnetized plasma is the ratio of the electron plasma frequency to the electron nonrelativistic gyrofrequency:

$$\alpha = \omega_{pe}/\Omega_e = 3.2\left(n_e/10^{10} \text{ cm}^{-3}\right)^{1/2}(B_0/100 \text{ G})^{-1}, \quad (3)$$

where $\Omega_e = (eB_0)/(m_e c)$ and e and m_e are the elemental charge unit and the electron mass, respectively. The value of α is small for a strongly magnetized plasma.

A particle with a velocity βc (Lorentz factor γ) and a pitch-angle cosine μ interacts most strongly with waves satisfying the resonance condition:

$$\omega - k_\| \beta\mu = \frac{n\omega_i}{\gamma}, \quad (4)$$

where n is for the harmonics of the gyrofrequency (not to be confused with the background particle number densities n_i), ω and $k_\|$ are the wave frequency and the parallel component of the wavevector in units of Ω_e and Ω_e/c, respectively (we use these units in the following discussion unless specified otherwise and in our case $k_\| = k$ and $n = -1$), and $\omega_i = q_i m_e/e m_i$ are the particle gyrofrequencies in units of Ω_e; $\omega_e = -1$ for electrons and $\omega_p = \delta \equiv m_e/m_p$ for protons, where m_p is the proton mass (for more details see also DP94). One notes that low-energy particles mostly resonate with waves with high wavenumbers and only relativistic particles interact with large-scale waves with low frequencies. The resonant wave-particle interaction can transfer energy between the turbulence and particles with the details depending on the particle distribution and the spectrum and polarization of the turbulence.

2.3. Fokker-Planck Coefficients

The evaluation of the F-P coefficients requires a knowledge of the spectrum of the turbulence. Following previous studies (DP94; PP97), we first assume a power-law distribution of unpolarized turbulent plasma waves. For unpolarized turbulence, the amplitudes of the waves only depend on k. Then we have $\mathcal{E}(k) = (q-1)\mathcal{E}_{\text{tot}} k_{\min}^{q-1} k^{-q}$ for $k > k_{\min}$ (i.e., a large-scale cutoff), where the turbulence spectral index $q > 1$. For a given turbulence energy density $\mathcal{E}_{\text{tot}}$, $k_{\min}$, presumably larger than the inverse of the size of the acceleration region, determines the maximum energy that the accelerated particles can reach and the characteristic timescale of the interaction. The general features of this situation have been explored in the papers cited above. For the sake of completeness, we briefly summarize the key results here.

The F-P coefficients can be written as

$$D_{ab} = \frac{(\mu^{-2}-1)}{\tau_{pi}\gamma^2} \sum_{j=1}^{N} \chi(k_j) \begin{cases} \mu\mu(1-x_j)^2 & \text{for } ab = \mu\mu, \\ \mu p x_j(1-x_j) & \text{for } ab = \mu p, \\ p^2 x_j^2 & \text{for } ab = pp, \end{cases} \quad (5)$$

where

$$\chi(k_j) = \frac{|k_j|^{-q}}{|\beta\mu - \beta_g(k_j)|}, \quad x_j = \mu\omega_j/\beta k_j. \quad (6)$$

The sum over j is for the resonant interactions discussed in the previous section. The characteristic interaction timescale for each of the charged particle species is $\tau_{pi} = \tau_p/\omega_i^2$ with that for electrons given by (see DP94)

$$\tau_p^{-1} = \frac{\pi}{2}\Omega_e\left(\frac{\mathcal{E}_{\text{tot}}}{B_0^2/8\pi}\right)(q-1)k_{\min}^{q-1}. \quad (7)$$

In general, the F-P coefficients have complicated dependence on the turbulence spectral index q, the plasma parameter α, and the energy and pitch angle of the particles. The exact solution of the full F-P equation is a difficult task. Fortunately, under certain conditions considerable simplifications are possible. These conditions are defined by the relative values of the three F-P coefficients. The pitch-angle change rate of the particles is proportional to $D_{\mu\mu}$, while the momentum or energy change rate is proportional to D_{pp}/p^2. As evident from equation (5), the behavior of $D_{\mu p}/p$ is intermediate between the two.

2.4. Diffusion-Convection Equation

The relative values of the F-P coefficients determine the type of approximations that can be used for solving the F-P equation. We now show that for most conditions reasonable approximations lead to the well-known transport equation (eq. [10]). In order to justify these approximations, it is convenient to define two ratios of the coefficients:

$$R_1(\mu,p) = \frac{D_{pp}}{p^2 D_{\mu\mu}}, \quad (8)$$

$$R_2(\mu,p) = \frac{D_{p\mu}}{p D_{\mu\mu}}. \quad (9)$$

We show in the following sections for most energies and pitch angles both R_1 and $|R_2| \ll 1$, which means that $D_{\mu\mu} \gg D_{pp}/p^2$. Under these conditions the particles are scattered frequently before being significantly accelerated and the accelerated particle distribution is nearly isotropic. Then the pitch-angle–averaged particle distribution function $F(s,t,p) = 0.5\int_{-1}^{1} d\mu f(\mu,s,t,p)$ satisfies the well-known diffusion-convection equation (see, e.g., Kirk et al. 1988; DP94; PP97).

In this study we are interested in the relative acceleration of electrons and protons that is not sensitive to the detailed geometry or the inhomogeneities of the source. Therefore, we can assume a homogeneous and finite (size L) source or alternatively confine our discussion to spatially integrated spectra. In this case we can treat the spatial diffusion or advection of the particles by an energy-dependent escape term. Then the above-mentioned equation is reduced to

$$\frac{\partial N}{\partial t} = \frac{\partial^2}{\partial E^2}(D_{EE}N) + \frac{\partial}{\partial E}\left[(\dot{E}_L - A)N\right] - \frac{N}{T_{\text{esc}}} + Q, \quad (10)$$

where $E = (\gamma-1)m_i c^2$ is the particle kinetic energy, $N(t,E)\,dE = 4\pi p^2\,dp\int_0^L F(s,t,p)\,ds$, $\dot{E}_L$ describes the net systematic energy loss, and $Q(t,E) = 0.5\int_{-1}^{1} d\mu\int_0^L S(s,\mu,t,E)\,ds$ is the total injection flux of particles into the acceleration region. The term D_{EE} describing the diffusion in energy is

related to D_{pp} and defines the acceleration time, and $T_{\rm esc}$ is related to the scattering time $\tau_{\rm sc}$:

$$T_{\rm esc} = \frac{L^2/v^2}{\tau_{\rm sc}}, \quad \tau_{\rm sc} = \frac{1}{2}\int_{-1}^{1} d\mu \, \frac{(1-\mu^2)^2}{D_{\mu\mu}} \ll L/v, \quad (11)$$

$$\tau_{\rm ac} = \frac{E^2}{D_{EE}}, \quad D_{EE} = \frac{E^2}{2}\int_{-1}^{1} d\mu \, D_{\mu\mu}\left(R_1 - R_2^2\right). \quad (12)$$

Note that equation (10) describes the energy diffusion with two terms, D_{EE} and the direct acceleration rate:

$$A(E) = \frac{1}{\beta\gamma^2}\frac{d\beta\gamma^2 D_{EE}}{dE} = \frac{dD_{EE}}{dE} + \frac{D_{EE}}{E}\frac{2-\gamma^{-2}}{1+\gamma^{-1}}. \quad (13)$$

There are several important features in the diffusion coefficients that we emphasize here:

1. The first is that in the *extremely relativistic limit* the diffusion coefficients (and their ratios) for protons and electrons are identical and assume asymptotic values such that both of the ratios are much less than 1. Therefore, equations (10), (11), and (12) are valid. (Strictly speaking, this is not true for very strongly magnetized plasmas $\alpha \le \delta^{1/2}$ where one gets $R_1 \sim |R_2| \sim 1$; see eq. [5].)

2. The second is that *at low energies*, as pointed out by PP97, R_1 and R_2^2 are not necessarily less than 1, especially for plasmas with low values of α. In the extreme case of $R_1 \gg |R_2| \gg 1$, three of the four diffusion terms in equation (1) can be ignored. Again, if we assume a finite homogeneous region or integrate over a finite inhomogeneous source, the resultant equation becomes similar to equation (10). Now because of the lower rate of pitch-angle scatterings, the escape time may be equal to the transit time $T_{\rm esc} \sim L/(v\mu)$, the other transport coefficients D_{EE} and $\dot{E}_L$ (and consequently the accelerated particle spectra) may depend on the pitch angle, and the assumption of isotropy may not be valid. However, as can be seen in the next section (Figs. 5 and 6), these coefficients change slowly with μ, except for some negligibly small ranges of μ, so that the expected anisotropy is small. In addition, at lower energies Coulomb scatterings become increasingly important and can make the particle distribution isotropic. In many cases, especially for plasmas not completely dominated by the magnetic field (i.e., for $\alpha \ge 1$), one can neglect the small expected anisotropy and integrate the equation over the pitch angle, in which case the transport equation becomes identical to equation (10) except now

$$T_{\rm esc} = L/\sqrt{2}v \ll \tau_{\rm sc} \sim \langle 1/D_{\mu\mu}\rangle, \quad (14)$$

$$\tau_{\rm ac} = \frac{2p^2}{\int_{-1}^{1} d\mu \, D_{pp}(\mu)}, \quad (15)$$

where angle brackets denote averaging over the pitch angle.

3. It is easy to see that one can combine the above two sets of expressions (eqs. [11]–[15]) for the acceleration rates (or timescales) and the escape times at the nonrelativistic and extremely relativistic cases as

$$T_{\rm esc} = \frac{L}{\sqrt{2}v}\left(1 + \frac{\sqrt{2}L}{v\tau_{\rm sc}}\right), \quad \tau_{\rm ac} = \frac{E^2}{D_{EE}}, \quad (16)$$

and

$$D_{EE} = \frac{E^2}{2}\int_{-1}^{1} d\mu \, D_{\mu\mu}\begin{cases} R_1 & \text{if } R_1 \gg |R_2| \gg 1, \\ R_1 - R_2^2 & \text{if } R_1, |R_2| \ll 1 \end{cases} \quad (17)$$

The first expression in equation (17) is valid at low values of E and α and the second at higher energies and in weakly magnetized plasmas. However, it turns out that at extremely relativistic energies and in weakly magnetized plasmas ($\alpha > 1$), independent of other conditions, $R_2^2 \ll R_1$ and the first expression can be used. These expressions and equation (10) then describe the problem adequately for most purposes in high-energy astrophysics, in particular for solar flares, the focus of this paper.

4. Finally, in certain cases, especially in the intermediate energy range, the quantity $R_1 - R_2^2$ appearing in equations (12) and (17) can be small. The acceleration rate can be reduced dramatically when both R_1 and $|R_2|$ are much less than 1 and $R_1 \simeq R_2^2$. From the definitions of these ratios and expressions for the F-P coefficients (eqs. [8], [9], and [5]) it is clear that if there were only one resonant interaction, one would have $R_1 = R_2^2$ and there would be no acceleration. Thus, strictly speaking, the use of equation (10) with interactions involving only one wave mode (say the Alfvén) is incorrect. However, as we show in § 3.1, there are always at least two resonant interactions in unpolarized turbulence, in which case $R_1 \ne R_2^2$ so that the acceleration rate is finite. But if one of the interactions is much stronger than the others, $R_1 - R_2^2$ can be small. In the next section we show some examples where this is true (Fig. 5) and that this happens at the intermediate values of energy (Fig. 6). The acceleration rate is then reduced greatly. The much lower acceleration rate at the intermediate energies compared to the higher rates in the nonrelativistic and extremely relativistic limits introduces an acceleration barrier. As we shall see, in the intermediate energy range the behaviors of protons and electrons are quite different and a much stronger acceleration barrier appears for protons.

2.5. Loss Rate

To determine the distributions of the accelerated protons and electrons by solving equation (10) with the above formalism, in addition to the transport coefficients D_{EE}, A, and $T_{\rm esc}$, we need to specify the loss term $\dot{E}_L$. For electrons the loss processes are dominated by Coulomb collisions at low energies and by synchrotron losses at high energies:

$$\dot{E}_{Le} = 4r_0^2 m_e c^3\left(\pi n_e \ln\Lambda/\beta + B_0^2\beta^2\gamma^2/9m_e c^2\right), \quad (18)$$

where $r_0 = 2.8\times10^{-13}$ cm is the classical electron radius and $\ln\Lambda = 20$ is a reasonable value in our case (See Leach 1984). The ion losses in a fully ionized plasma are mainly due to Coulomb collisions with the background electrons and protons (Post 1956; Ginzburg & Syrovatskii 1964). For electron-ion collisions, we have

$$\dot{E}_{Li} = 2\pi r_0^2 m_e c^3 n_e\left(\frac{q_i}{e}\right)^2$$

$$\times\begin{cases} 2\sqrt{2}\beta^2\beta_{Te}^{-3}\ln\Lambda\left(\dfrac{3}{\pi}\right)^{1/2} & \text{for } \beta < \beta_{Te}, \\[2ex] \beta^{-1}\ln\left(\dfrac{m_e^2 c^2\beta^4}{\pi r_0 n_e\hbar^2}\right) & \text{for } 1 \gg \beta > \beta_{Te}, \\[2ex] \ln\left(\dfrac{m_e^2 c^2\gamma^2}{2\pi r_0 n_e\hbar^2}\right) & \text{for } \dfrac{m_i}{m_e} \gg \gamma \gg 1, \\[2ex] \ln\left(\dfrac{m_e m_i c^2\gamma}{4\pi r_0 n_e\hbar^2}\right) & \text{for } \gamma \gg \dfrac{m_i}{m_e}, \end{cases} \quad (19)$$

where $\beta_{Te} = (3k_B T_e/m_e c^2)^{1/2}$ is the mean thermal velocity of the background electrons in units of c and k_B is the Boltzmann constant. For proton-ion collisions, which are important for ions with even lower energies, we have (Spitzer 1956)

$$\dot{E}_{Li} = 4\pi r_0^2 m_e c^3 n_p (q_i/e)^2 (m_e/m_p) \beta^{-1} \ln \Lambda. \qquad (20)$$

These loss processes dominate at different energies, and we can define a loss time $\tau_{\mathrm{loss}} = E/\dot{E}_L$.

2.6. Steady State Solution and Normalization

We use the impulsive phase conditions of solar flares for our demonstration. In this case, we can assume that the system is in a steady state because the relevant timescales are shorter than the dynamical time (the flare duration). We also assume the presence of a constant spectrum of turbulence. We are interested in the acceleration from a thermal background plasma; therefore, a thermal distribution is assumed for the source term Q. As described above, equation (10) may not be valid at low (keV) energies where $R_1 \gg 1$. However, for solar flare conditions and in the keV energy range, Coulomb scatterings become important ($D_{\mu\mu}^{\mathrm{Coul}} \gg D_{\mu\mu}^{\mathrm{wave}}$; see Hamilton & Petrosian 1992). In this case $R_1 \ll 1$ and the particle distribution will be nearly isotropic at all energies. We therefore calculate the acceleration rate with the second expression of equation (17) and solve equation (10) to get the distributions of the accelerated particles over all energies.

To appreciate the relevant physical processes, one can compare the acceleration time with the escape and the loss time. We are mostly interested in the energy range above the energy of the injected particles. Thus, the source term is not as important in shaping the spectrum as the other terms. In the energy band where the escape and loss terms are negligible, from the flux conservation in the energy space, one can show that $AN - d(D_{EE}N)/dE = \mathrm{const}$. On the other hand, when the acceleration terms are negligible, no acceleration occurs. When the escape time becomes much shorter than the acceleration time and both of them are much shorter than the loss time, particles escape before being accelerated. This results in a sharp cutoff in the particle distribution at the energy where $T_{\mathrm{esc}} \simeq E/A(E) \sim E^2/D_{EE}$. When the escape time is long and the loss time is much shorter than the acceleration time, one would then expect a quasi-thermal distribution for the Coulomb collisional losses (Hamilton & Petrosian 1992) and a sharp high-energy cutoff for the synchrotron losses (Park et al. 1997). Power-law distributions can be produced only in energy ranges where the loss term is small and the acceleration and escape times have similar energy dependence.

The normalization of the steady state particle distributions is determined by their rates of acceleration, escape, and injection. The injection rates depend on the geometries of the reconnection and the turbulent acceleration site and on possible contributions of the charged particles to reverse currents that must exist when a net charge current leaves the acceleration site. A more detailed time-dependent treatment is required to determine the relative normalization. This is beyond the scope of the paper and will be dealt with in the future. Here we concentrate on the relative shapes of the electron and proton spectra in the LT and FP sources. We assume that the injection flux $\int Q \, dE = 1 \mathrm{\ s^{-1} \ cm^{-2}}$ for both electrons and protons (see also § 5). In the steady state this is equal to the flux of the escaping particles $N_{\mathrm{esc}}^{\mathrm{tot}} = \int_0^\infty N_{\mathrm{LT}}(E)/T_{\mathrm{esc}}(E) \, dE$. Since the escaping particles lose most of their energy at the

FPs, instead of $N_{\mathrm{esc}}(E) = N_{\mathrm{LT}}(E)/T_{\mathrm{esc}}(E)$ we show the effective particle distribution for a thick target (complete cooling) FP source, which is related to the corresponding LT distribution N_{LT} via (Petrosian & Donaghy 1999)

$$N_{\mathrm{FP}}(E) = \frac{1}{\dot{E}_L} \int_E^\infty \frac{N_{\mathrm{LT}}(E')}{T_{\mathrm{esc}}(E')} \, dE'. \qquad (21)$$

3. APPLICATION IN COLD HYDROGEN PLASMAS

In this section we describe the relative acceleration of electrons and protons in cold, fully ionized, pure hydrogen plasmas. This is an approximation because all astrophysical plasmas contain some helium and traces of heavy elements. Ignoring the effects of helium (trace elements will, in general, have no influence on the following discussion) and adopting a turbulence spectrum of a single power law of the wavenumber simplify the mathematics and allow us to demonstrate the differences between the acceleration rates of electrons and protons more clearly. Moreover, in some low-temperature plasmas, most of the helium may be neutral and not be involved in the SA processes. The results presented here are a good approximation. Pure hydrogen plasmas can also be realized in terrestrial experiments to test the theory. The formalism can also be easily generalized to the case of electron-positron plasmas and to more complicated situations. In the next section we present our results for plasmas including about 8% by number of helium and for turbulence with a more realistic spectrum.

3.1. Dispersion Relation and Resonant Interactions

In a pure hydrogen plasma, equation (2) reduces to (PP97)

$$\frac{k^2}{\omega^2} = 1 - \frac{\alpha^2(1+\delta)}{(\omega-1)(\omega+\delta)}, \qquad (22)$$

and the Alfvén velocity in units of c is given by $\beta_A = \delta^{1/2}/\alpha$. (For $e^\pm$ pair-dominated plasmas $\delta = 1$).

The left panels of Figure 1 depict the normal modes of these waves, which compose four distinct branches. From top to bottom in the top left panel, we have the electromagnetic wave branch (EM; long-dashed line), electron-cyclotron branch (EC; dot-dashed line), proton-cyclotron branch (PC; dotted line), and a second electromagnetic wave branch (EM'; short-dashed line). The bottom left panel is an enlargement of the region near the origin. The positive and negative frequencies mean that the waves are right- and left-handed polarized, respectively, where the polarization is defined relative to the large-scale magnetic field (Schlickeiser 2002). The right panels of Figure 1 depict the group velocities $\beta_g = d\omega/dk$ of these waves. One may note that the signs of the phase velocity $\beta_{\mathrm{ph}} = \omega/k$ and the group velocity of a specific wave mode are always the same.

In the left panels of Figure 1, the two solid straight lines depict equation (4) for an electron (upper line) and a proton (lower line) with $\beta = 0.5$ and $\mu = 0.25$. The intersections of these lines with the wave branches satisfy the resonance condition. The electron interacts resonantly at the indicated point with the EC branch and at another point with the PC branch at a high negative wavenumber that lies outside the figure. The proton, on the other hand, resonates with not only one PC wave but also three EC waves (only two of which are seen in the bottom left panel of the figure). As we show below, the fact that certain protons can resonate with more than one
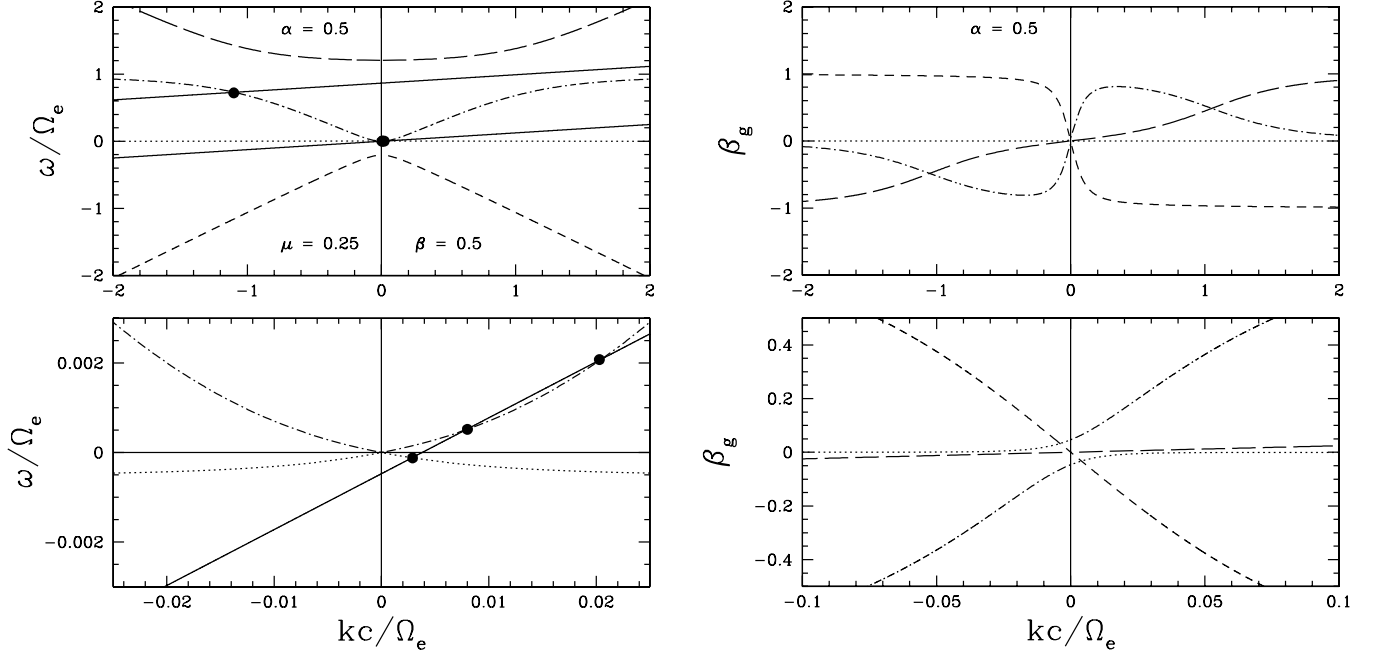
Fig. 1.—*Left*: Dispersion relation of parallel-propagating waves in a cold pure hydrogen plasma with $\alpha = 0.5$. The bottom left panel is an enlargement of the region around the origin. The lines, from top to bottom, describe the EM (*long-dashed line*), EC (*dot-dashed line*), PC (*dotted line*), and EM′ (*short-dashed line*) waves. The upper and lower solid lines give, respectively, the resonance conditions for electrons and protons with $v = 0.5c$ ($\beta = v/c$) and $\mu = 0.25$. Resonant interactions occur at the points where these lines cross the lines that depict the waves. *Right*: Same as the left panels, but for the group velocity $\beta_g = d\omega/dk$ vs. the wavenumber k. The line type remains the same for each wave branch. Negative group velocities mean that the energy fluxes of the waves are in the direction antiparallel to the large-scale magnetic field. [*See the electronic edition of the Journal for a color version of this figure.*]

EC wave has significant implications for the overall proton acceleration process.

3.2. *Critical Angles and Critical Velocities*

In general one expects four resonant points. However, for a given particle velocity or energy, at *critical angles*, where the group velocities of the waves are equal to the parallel component of the particle velocity, the number of resonant points can change from four to two or vice versa. Figure 2 shows the velocity dependence of the critical angles for electrons (*top*) and protons (*bottom*) in plasmas with $\alpha = 0.5$ (*left*) and 0.1 (*right*). (The results for electrons are the same as those given by PP97.) Both particles have at least two resonant interactions (one with the PC and one with the EC branch except for $\mu = 0$ where electrons interact with two EC waves and protons interact with two PC waves).

Electrons with a large μ can have two additional resonances with the EM branch, and those with a small μ have two additional resonances with the EC branch. The two regions with four resonances grow with decreasing α and shrink as α increases. For larger values of α the interaction is weaker because for large ranges of velocities and pitch angles electrons interact with only two waves (e.g., the interactions with the EM branch disappear for $\alpha > 1$; see Figs. 2 and 3). But as α approaches zero, the region with two wave interactions diminishes and the two lines for the critical angles merge into one, satisfying the relation

$$\mu_{\rm cr} = (\gamma - 1)/\beta\gamma \quad \text{for } \alpha \to 0. \tag{23}$$

In this case there are always four resonances and the total interaction is strong at all energies.

Protons have a similar, but slightly more complicated, behavior. As μ increases, one obtains interactions with 1EC+3PC,

1EC+1PC, 3EC+1PC, and back to 1EC+1PC waves. With the decrease of α, the upper two regions diminish, while the lower portions increase in size. Protons can also be accelerated by the EM′ waves, but this only occurs in more highly magnetized plasmas ($\alpha < \delta^{1/2}/2 \sim 0.012$) as compared with the interactions of electrons with the EM branch. At such low values of α a region with four interactions (1EC+1PC+2EM′) appears in the upper portion of the μ-β plane and its lower boundary eventually merges with the lower line for $\mu_{\rm cr}$ as α approaches zero. Just like electrons, the critical angle is given by equation (23). In this limit, particles are basically exchanging energy with the Poynting fluxes of the electromagnetic waves.

These behaviors can also be seen in Figure 3, where instead of $\mu_{\rm cr}$ we plot what one may call the *critical velocities* as a function of α for two values of μ. Note that in the proton panel with $\mu = 1.0$ there is a small region with $\alpha < 0.012$ where there are four resonances, including two with the forward-moving left-handed polarized electromagnetic waves from the EM′ branch. Protons will not resonate with the electromagnetic waves for larger values of α. In general, we have similar patterns of transition between different regions caused by the electromagnetic branches in the μ-β space, except that the transitions for protons occur at a value of α that is lower than that for electrons by a factor of $\delta^{1/2}$. The main difference in the behaviors of electrons and protons resides in their four resonant interactions with the PC and EC branches. Protons have two such regions where they resonate with "1EC+3PC" or "3EC+1PC," while electrons only have one with "3EC+1PC"; electrons never interact with more than one PC wave. This is where the above scaling symmetry of α between protons and electrons is broken.

Low-energy approximations.—Because the acceleration of particles at low energies is of particular interest, we present
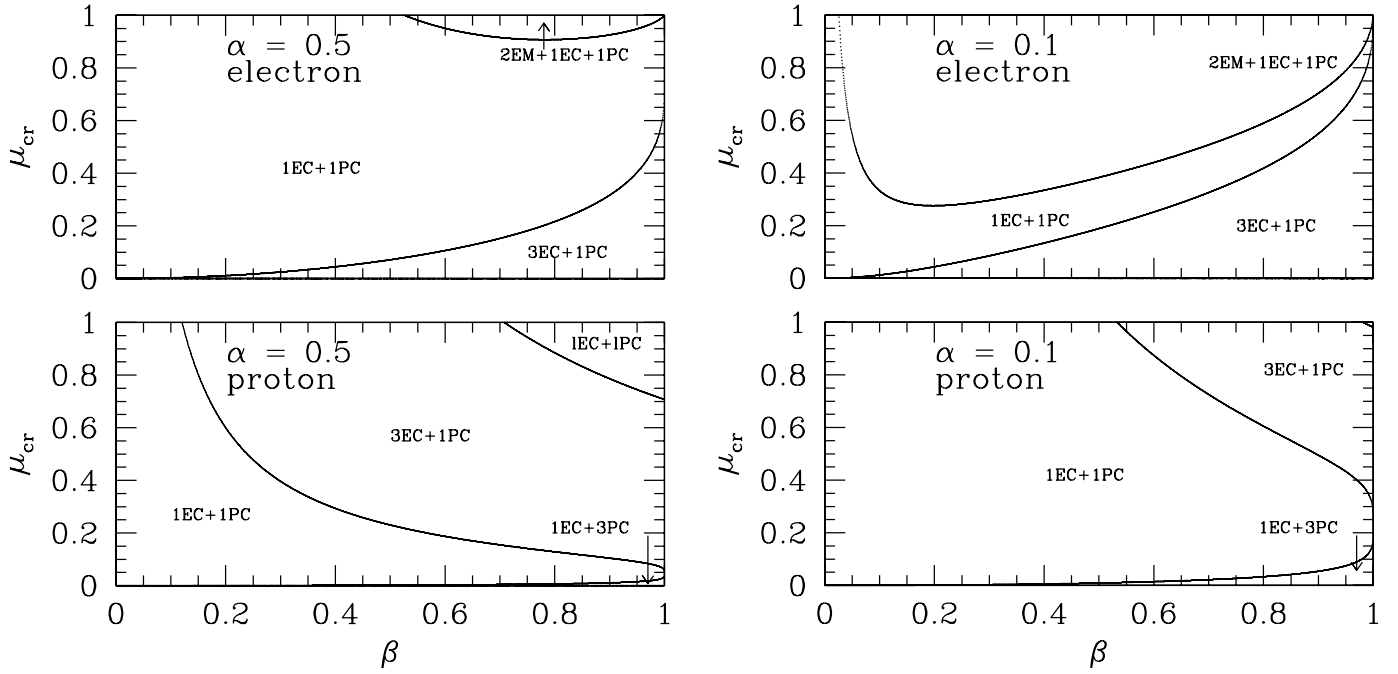
Fig. 2.—*Left*: Velocity dependence of the critical angles in a plasma with $\alpha = 0.5$ for electrons (*top*) and protons (*bottom*). At small pitch angles, i.e., $\mu \to 1$, electrons can resonate with high-frequency electromagnetic waves of the EM branch (region labeled "2EM+1EC+1PC"), while energetic protons mainly interact with the Whistler and Alfvén waves (region labeled "3EC+1PC"). *Right*: Same as the left panels, but for $\alpha = 0.1$ where interactions of protons with the Whistler waves start at a higher energy. See text for details.

here some approximate analytic relations, which are derived in Appendices A, B, C, and D.

The first is for the proton critical velocity line dividing the region with two and four resonances (i.e., the middle line in the bottom left panel of Fig. 3). As can be seen in the following sections, at a given α the acceleration rate (eq. [17]) increases dramatically once protons attain the critical velocity or energy and enter the region with four resonant interactions. The pitch-angle–averaged acceleration rate also increases

sharply above this energy. It will be useful to have a formula to estimate this critical velocity. We find the following approximate expression for this transition:

$$\beta_{cr} = \frac{0.06\alpha}{0.0012 + \alpha^2},$$

$$\text{or } E_{cr} = \frac{1}{2} m_p c^2 \beta_{cr}^2 = 1.7 \text{ MeV} \left(\frac{\alpha}{0.0012 + \alpha^2}\right)^2, \quad (24)$$

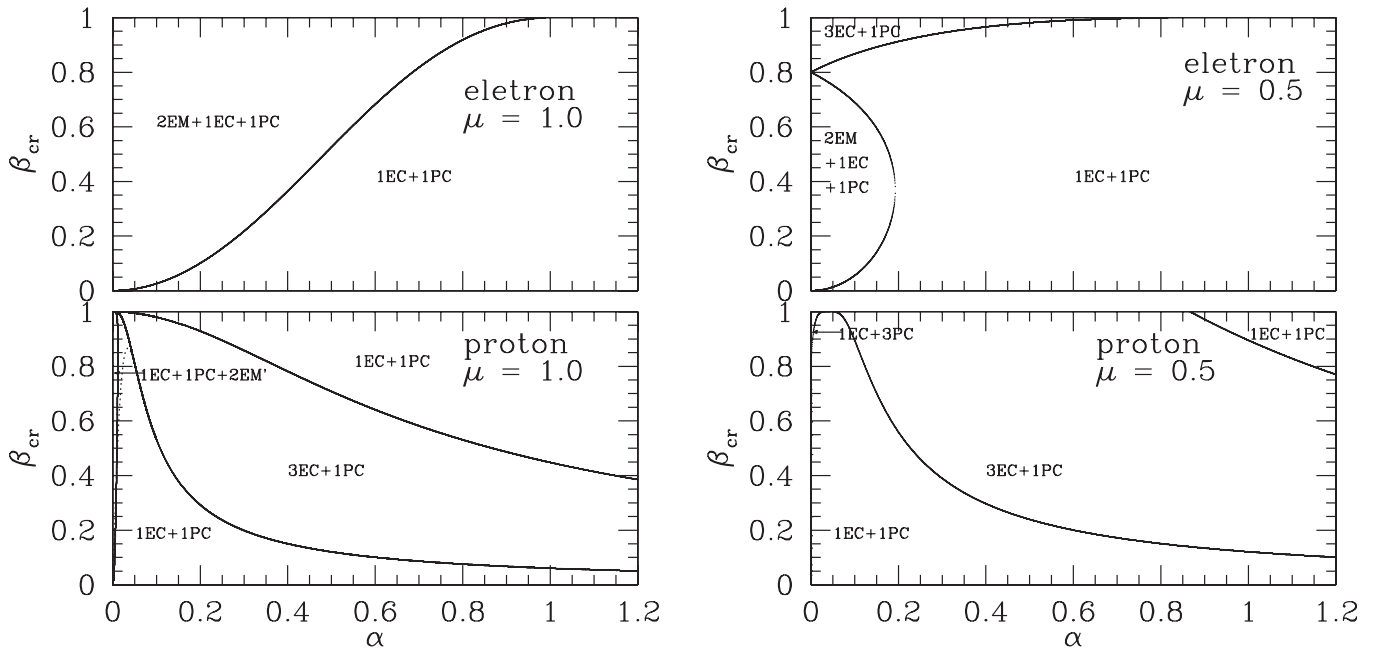Fig. 3.—Same as Fig. 2, but depicting the dependence of the critical velocities on the plasma parameter α. Combining this with Fig. 2, one can tell the wave branches responsible for the critical velocities. [*See the electronic edition of the Journal for a color version of the left panels of Fig. 3.*]
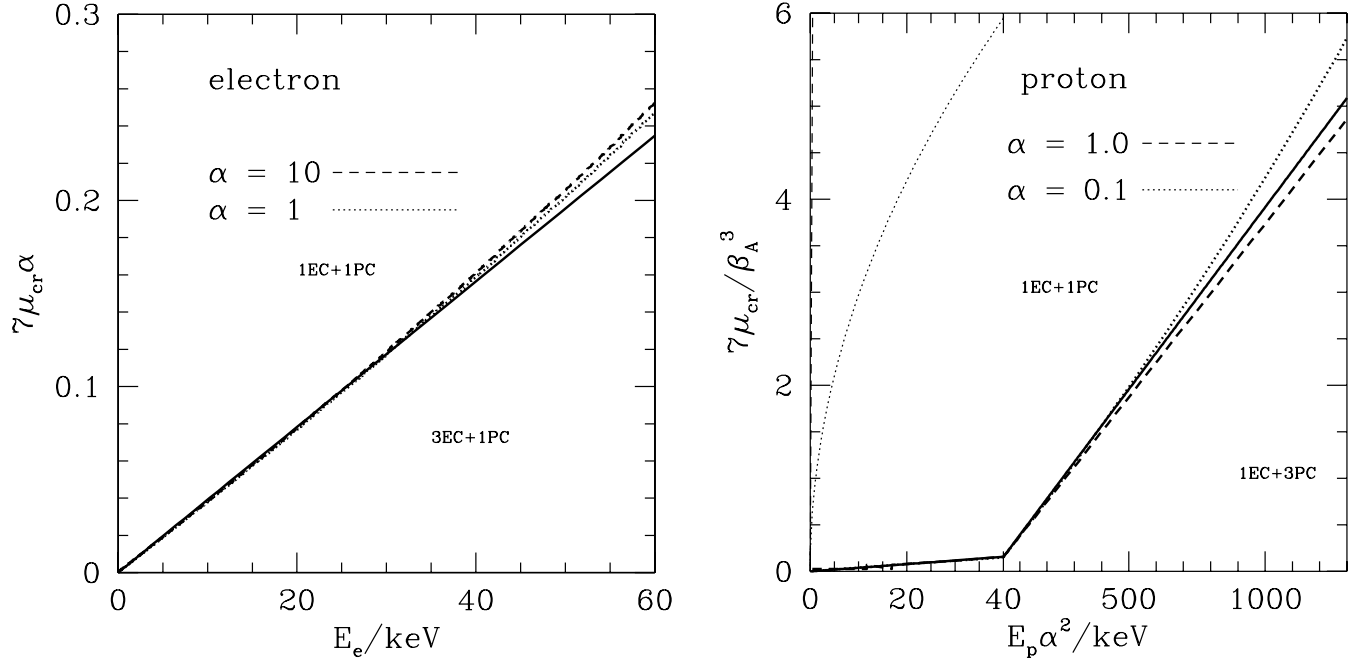
Fɪɢ. 4.—Comparison of the analytical expressions (eq. [25]; *solid lines*) with the exact values of $\mu_{\rm cr}$ (*dotted and dashed lines*; in the low energy range) due to resonant interactions with the EC (*left*, for electrons) or PC (*right*, for protons; note that the region to the left of $E_p\alpha^2 = 40$ keV has an expanded scale) branch. The thin dashed (barely visible near the left axis and for $\alpha = 1.0$) and dotted (for $\alpha = 0.1$) lines in the right panel give the critical angles for waves obeying the Alfvénic dispersion relation $\omega = -|k|\beta_{\rm A}$, which clearly give incorrect descriptions for the acceleration of low-energy protons. Low-energy electrons do not interact with the Alfvén waves.

which is shown by the dotted line in the bottom left panel of Figure 3 and agrees within 0.2% with the exact result for $\alpha > 0.05$.

The second approximation is for the critical angles of protons below the critical energy (velocity) and low-energy electrons, most of which interact only with two waves with one dominating over the other. When this happens, the acceleration rate for the particles can be very small (see § 2.3). Only particles with very large pitch angles ($\mu \simeq 0$) have four resonances and significant contributions to the pitch-angle–averaged acceleration rate. The regions for this lie in the small areas below the lowest lines in Figure 2, which are barely visible for the proton and $\alpha = 0.5$ case. As shown in Appendices A and B using the approximations of equations (A1) and (A2) for the dispersion relations, we can derive analytic expressions for the critical angles, which in the nonrelativistic limit give $\mu_{\rm cr} \propto \beta^2 \propto E/mc^2$. Empirically, we find that the following simple approximate expressions, as shown in Figure 4, agree with the exact results to better than $\sim$10% in the indicated energy ranges:

$$\mu_{\rm cr} = \frac{1}{3.5\alpha} \begin{cases} \delta^{1/2}E/m_pc^2 & \text{for protons; } E < E_{\rm cr}, \\ E/m_ec^2 & \text{for electrons; } E < 60 \text{ keV.} \end{cases} \quad (25)$$

Here it should be emphasized that the commonly used approximation of accelerating protons by the Alfvén waves with the dispersion relation $\omega = -|k|\beta_{\rm A}$ for $|\omega| < \delta$, which is valid at relativistic energies (Barbosa 1979; Schlickeiser 1989; Miller & Roberts 1995), is invalid at low energies. This can be seen from the bottom left panel of Figure 1, which shows clearly that the dispersion relation of the waves in resonance with low-energy protons deviates far from the simple Alfvénic form. For the simple Alfvénic dispersion relation, nonrelativistic protons resonate with both a forward- and a backward-

moving wave only if $|\mu| < \mu_{\rm cr} = \beta_{\rm A}(\gamma - 1)/\beta\gamma$. (Particles only interacting with one wave cannot be accelerated; see § 2.4.) This critical angle is indicated by the thin dashed (barely visible near the vertical axis) and dotted lines in the right panel of Figure 4 for $\alpha = 1.0$ and 0.1, respectively, which clearly overestimate by several orders of magnitude the fractions of low-energy protons that can be accelerated. The inefficiency of proton acceleration at intermediate energies, combined with the increase of the interaction rate above $E_{\rm cr}$, gives rise to the acceleration barrier to be described in § 3.4.

In most of the particle acceleration models, an injection process of high-energy particles is postulated as an input. If the injected particles have an energy above $E_{\rm cr}$, it may be appropriate to use the Alfvénic dispersion relation to describe the waves. If the energy of the injected particles is low, as is the case under study here, one must use the exact dispersion relation to calculate the acceleration of low-energy particles. Although most of the turbulence energy is carried by waves with low wavenumbers, the acceleration of low-energy particles is determined by waves with high wavenumbers (see eq. [4]), which can constrain the overall acceleration efficiency. As discussed above, the Alfvénic dispersion relation for the waves will overestimate the acceleration efficiency of low-energy protons significantly.

3.3. *Fokker-Planck Coefficients*

For a given power-law spectrum of the turbulence, it is straightforward to calculate the F-P coefficients with equation (5). Figure 5 shows variation of these coefficients with μ at some representative energies, and Figure 6 shows the variation of their inverses (i.e., times) with energy at different values of μ, here $\alpha = 0.5$ and $q = 1.6$. The discontinuous jumps occur at the critical values of $\mu_{\rm cr}$ and $\beta_{\rm cr}$ described in § 3.2. The
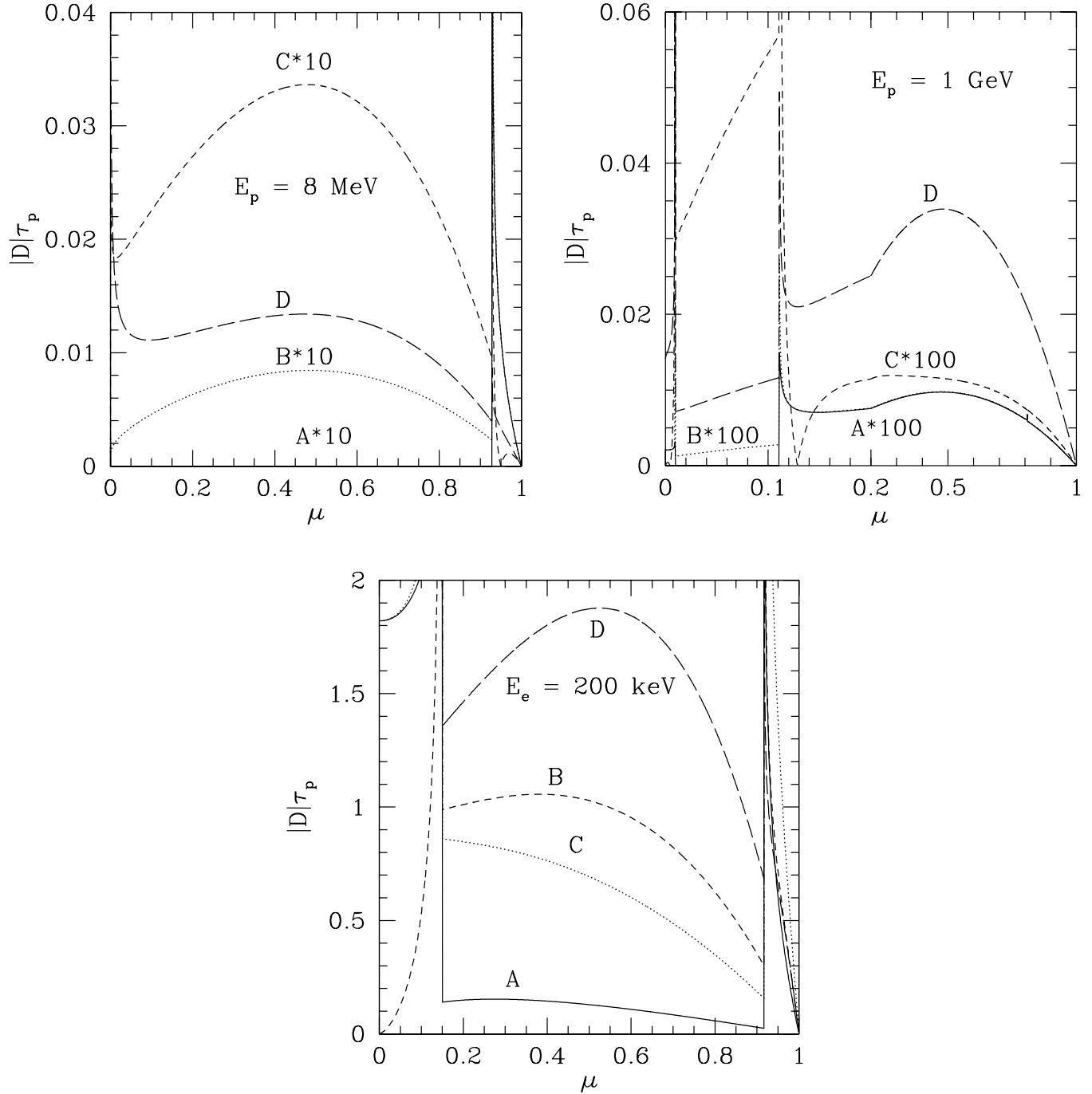
FIG. 5.—Pitch-angle dependence of the F-P coefficients (absolute values) for protons of two different energies (8 MeV, *left*; 1 GeV, *middle*) and 200 keV electrons (*right*). A, B, C, and D stand for $(D_{pp} - D^2_{p\mu}/D_{\mu\mu})/p^2$, D_{pp}/p^2, $|D_{p\mu}|/p$, and $D_{\mu\mu}$, respectively. The plasma parameter $\alpha = 0.5$ and the turbulence spectral index $q = 1.6$. Note that different coefficients are scaled differently and that, for illustration, in the middle panel the region to the left of $\mu = 0.2$ is expanded.

variations of the two ratios defined in equations (8) and (9) with energy at different pitch angles are shown in Figure 7. These results justify the discussion in § 2.4.

3.4. *Barrier in the Proton Acceleration*

In the previous section we showed that the pitch-angle–averaged acceleration rate is one of the dominating factors in the particle acceleration processes. The relative acceleration of protons and electrons therefore depends on the contrast of their acceleration times. Figure 2 shows that at low energies particles with $\mu > \mu_{cr}$ only resonate with one PC and one EC wave: the EC wave dominates the PC wave for electrons,

while the reverse is true for protons. These particles have significant contributions to the pitch-angle–averaged acceleration rate for $\mu_{cr} \ll 1$ (eq. [25]). Because the difference between the wavenumbers of the two waves interacting with protons is much larger than that for electrons, the resonant interaction is more strongly dominated by one of the resonant waves for protons than it is for electrons. The factor $1 - R^2_2/R_1$ for protons can therefore be several orders of magnitude smaller than that for electrons at a given energy and pitch angle (Fig. 6). Consequently, in the intermediate energies where $R_1 \sim R^2_2 \sim 1$, the pitch-angle–averaged acceleration time for protons has a more prominent increase than that
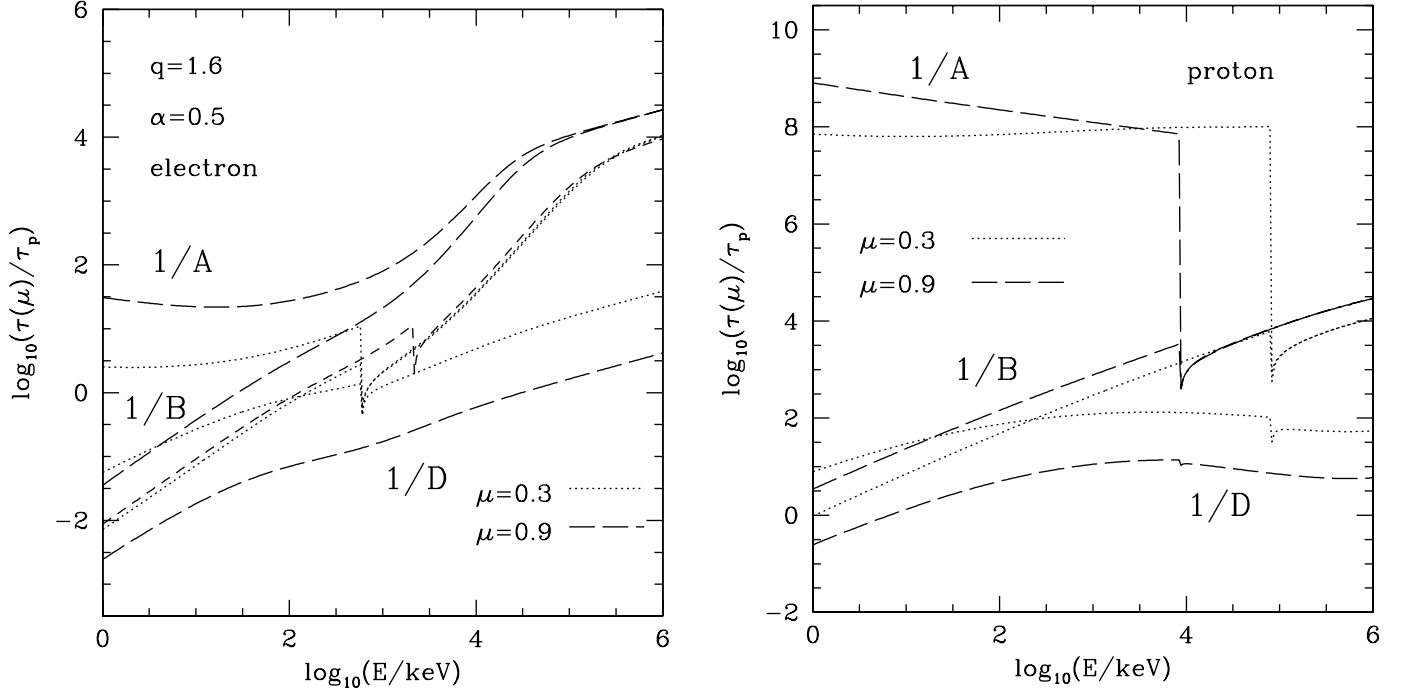
Fig. 6.—Energy dependence of the scattering, $1/D = D_{\mu\mu}^{-1}$, and acceleration times, $1/B = p^2/D_{pp}$ or $1/A = p^2/(D_{pp} - D_{\mu p}^2/D_{\mu\mu})$, in units of τ_p at different pitch angles for electrons (*left*) and protons (*right*). The plasma parameter $\alpha = 0.5$ and the turbulence spectral index $q = 1.6$. Note that $A = B$ for $\mu = 0$. At very low energies $D_{\mu\mu}^{-1} > p^2/D_{pp}$ and the acceleration time $\tau_{ac} = p^2/D_{pp}$. At intermediate and high energies $\tau_{ac} = p^2/(D_{pp} - D_{\mu p}^2/D_{\mu\mu})$. [*See the electronic edition of the Journal for a color version of this figure.*]

for electrons. At still higher energies, particles with four resonances dominate the acceleration rate because $R_2^2 \ll R_1$ for the interactions. For both electrons and protons, the new resonant wave modes come from the EC branch. In the relativistic limit, the acceleration is dominated by resonances with the Alfvén waves, and the interaction rates for electrons and protons become comparable.

Figure 8 shows the pitch-angle–averaged acceleration (*thick lines*) and scattering (*thin dashed lines*) times in units of τ_p for electrons (*lower lines*) and protons (*upper lines*) in plasmas with $\alpha = 0.5$ (*left*) and 0.1 (*right*). The turbulence spectral index $q = 1.6$ here. The acceleration times for both cases in equation (17) are plotted with the invalid segments shown by dotted lines. We see that the pitch-angle–averaged
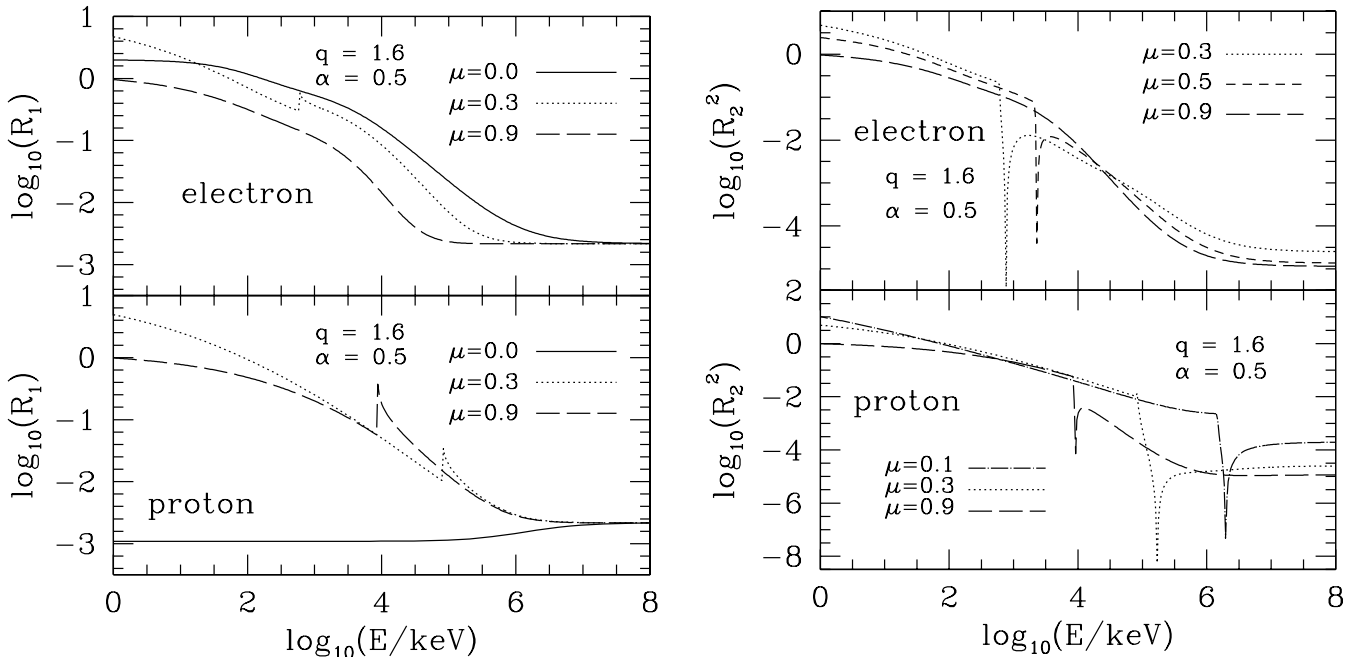

Fig. 7.—Ratios R_1 (*left*) and R_2^2 (*right*) as functions of energy for several different pitch angles for electrons (*top*) and protons (*bottom*). In general, R_1 and $|R_2|$ exceed unity at low energies and μ (and small values of α; see PP97). For protons, at certain ranges of E and μ, $R_2^2 \approx R_1 \ll 1$, and the acceleration rate, $D_{\mu\mu}(R_1 - R_2^2)$, can be very small (see eq. [12]).
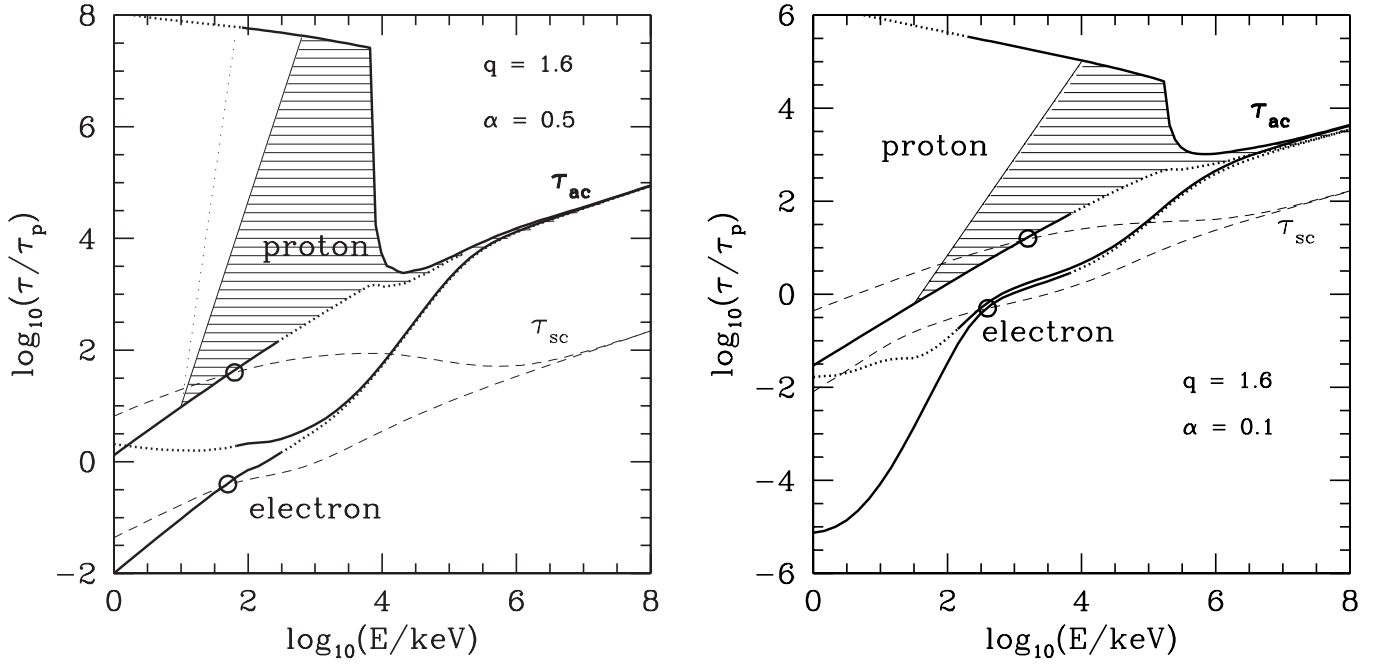
FIG. 8.—Pitch-angle–averaged acceleration (*thick lines*) and scattering (*thin dashed lines*) times in units of τ_p in plasmas with $\alpha = 0.5$ (*left*) and 0.1 (*right*). Here the turbulence spectral index $q = 1.6$. The acceleration times defined for both cases of eq. (17) are plotted with the corresponding invalid segments indicated by the dotted lines. The upper two lines are for protons and the lower two are for electrons. The circles indicate the points of transitions between low and high energies where $R_1 \sim |R_2| \sim 1$. The transitions of the electron acceleration times are quite smooth. The thin solid lines show schematically the transitions of the acceleration time for protons. The acceleration barrier (as indicated by the hatched areas) in the proton acceleration times is prominent. The sharp drop of the electron acceleration time with the decrease of energy for $\alpha = 0.1$ is due to interactions with the EM branch (PP97). [*See the electronic edition of the Journal for a color version of this figure.*]

acceleration times are much shorter than the corresponding scattering times for keV particles. The particle distributions can be anisotropic at these energies unless there are other scattering processes (e.g., Coulomb collisions). In the high-energy range, the scattering time is always shorter than the corresponding acceleration time when $\beta_A < 1$. The transitions where $R_1 \sim |R_2| \sim 1$ (as indicated by the circles in the figure) occur between 10^2 and 10^3 keV, increase with the decrease of α, and depend on the turbulence spectral index q as well.

There is clearly an acceleration barrier (as indicated by the shaded area) in the proton acceleration time. The thin solid line shows schematically the acceleration time of protons in the transition region. The sharp increase of the proton acceleration time at lower energies is caused by their low acceleration efficiency when the scattering rate already overtakes the acceleration rate as discussed above. The sharp drop of the proton acceleration time at a higher energy is due to interactions with the Whistler waves. Because protons with small pitch angles ($\mu \simeq 1$) interact with the Whistler waves at the lowest energy and the interaction is very efficient, this energy corresponds to the critical energy E_{cr} identified in equation (24).

These characteristics are not true for electrons. In § 3.2 we have shown that a small fraction of particles with $\mu < \mu_{cr}$ can resonate with four waves and $|R_2| \ll R_1$ for the interactions (Fig. 5). Compared with protons, more electrons can be accelerated this way (eq. [25]). Because the acceleration of electrons with two resonances is very inefficient, the acceleration of this small fraction of electrons already dominates the electron acceleration processes where the scattering rate becomes comparable with the acceleration rate. At even higher energies, there are no extra wave modes that can enhance the electron acceleration processes. Consequently, electrons have a smooth acceleration time profile.

Expressions for estimating the difference between electron and proton acceleration time are derived in Appendices A, B, C, and D. Briefly, because particles with $\mu < \mu_{cr}$ have significant contributions to the acceleration in the low-energy region ($\beta \ll 1$), one can estimate the pitch-angle–averaged acceleration times with the approximate expressions for the critical pitch angles (eq. [25]):

$$\frac{\tau_{ac}}{\tau_p} = 2 \left[\int_{-1}^{1} d\mu\, D_{\mu\mu} \left(R_1 - R_2^2 \right) \tau_p \right]^{-1}$$

$$\simeq 7\alpha^{q+2} \left(\frac{E}{m_e c^2} \right)^{(1-q)/2} \begin{cases} 1 & \text{for electrons,} \\ \delta^{-5/2} & \text{for protons,} \end{cases} \quad (26)$$

which is consistent with the numerical result within a factor of 2. In the relativistic limit ($\gamma \gg 1$), particles interact with the Alfvén waves and we find

$$\frac{\tau_{ac}}{\tau_p} = \frac{q(q+2)\alpha^2}{4\delta} \left(\frac{e}{q_i} \right)^{2-q} \left(\frac{E}{m_e c^2} \right)^{2-q}. \quad (27)$$

The difference between these two timescales at the critical energy (eq. [24]) gives an estimate of the height of the acceleration barrier.

3.5. *Application to Solar Flare Conditions*

Figure 9 shows a model of electron (*thick lines*) and proton (*thin lines*) acceleration in a strongly magnetized plasma. The LT size $L = 10^9$ cm, and the temperatures of the injected electrons and protons are the same, $k_B T = 1$ keV. The magnetic field and gas density are 400 G and 4.0×10^9 cm^{-3}, respectively, i.e., $\alpha = 0.5$ (see eq. [3]). The relevant timescales are shown in the left panel, where we have defined the
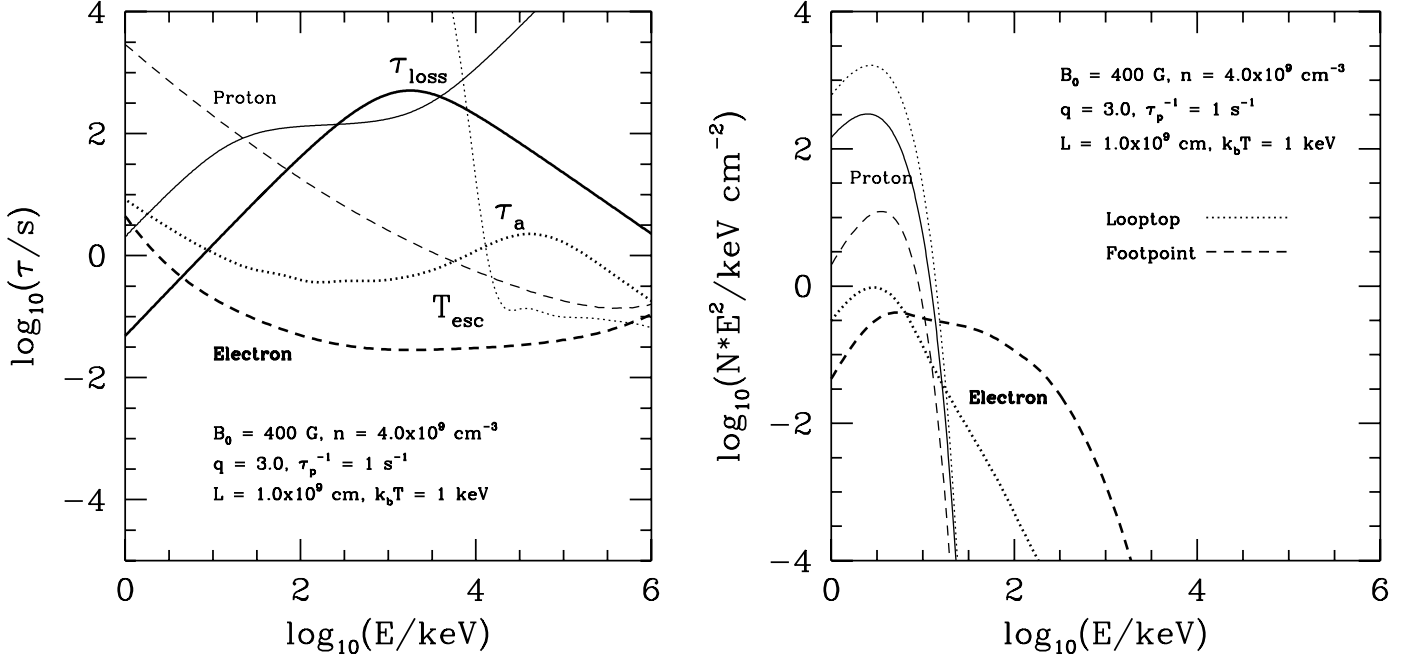
Fig. 9.—*Left*: Timescales for protons (*thin lines*) and electrons (*thick lines*) in a strongly magnetized plasma ($\alpha = 0.5$) with a steep turbulence spectrum ($q = 3$). The direct acceleration times $\tau_a = E/A$, which are related to the diffusion acceleration times τ_{ac}, are shown by the dotted lines. The solid lines are for τ_{loss}, and the dashed lines are for T_{esc}. *Right*: Corresponding distributions NE^2 of the accelerated electrons (*thick lines*) and protons (*thin lines*). Here the dotted lines give the thin target LT particle distributions, while the dashed lines indicate the effective thick target particle distributions at the FPs. The solid line gives the injected thermal particle distribution with arbitrary normalization. One can see that, because of the presence of the strong acceleration barrier (exceeding the range of the graph), protons are basically not accelerated. [*See the electronic edition of the Journal for a color version of this figure.*]

direct acceleration time $\tau_a = E/A$, which is related to τ_{ac} (eqs. [12] and [13]). The corresponding accelerated particle distributions are shown in the right panel. The dotted and dashed lines show the LT and FP spectra, respectively.

We note that for the above conditions the electrons can be accelerated to a few hundred keV while the proton acceleration is suppressed as a result of the acceleration barrier. The electron distribution steepens with the increase of energy because the escape time becomes shorter than the acceleration time ($T_{esc} < \tau_a$). At low energies where Coulomb collisions dominate, the LT electrons have a quasi-thermal distribution. The solid line gives the thermal distribution of the injected particles with arbitrary normalization. Because of the absence of acceleration at low energies, the steady state proton distributions are almost identical with the injected proton distribution.

To produce a near power-law electron distribution, as suggested by solar flare observations, the escape time must be comparable with the acceleration time in the relevant energy band. Because the escape time of the nonrelativistic electrons always decreases with the increase of energy, we adopt a turbulence spectral index of $q = 3$ in the model. The plasma time $\tau_p = 1$ s. Then we have the ratio of the turbulent wave energy density to the magnetic field energy density $8\pi\mathcal{E}_{tot}/B_0^2 = 4.4 \times 10^{-10}k_{min}^{-2}$. To ensure that this ratio is much less than 1 so that the quasi-linear approximation for the F-P treatment stays valid, one needs $k_{min} > 10^{-5}$ or an injection length of the turbulent waves of less than 10^6 cm (note that k_{min} is in units of $\Omega_e/c \simeq 0.24$ cm^{-1} here). Otherwise, the turbulence spectrum must flatten at low k so that there is less energy content in long-wavelength waves.

In §§ 3.2 and 3.4 we showed that the proton acceleration barrier moves toward lower energies with the increase of α.

Hence, in very weakly magnetized plasmas, this barrier can be close to the thermal energy of the injected particles and thus has little effect on the acceleration of protons. Protons can be accelerated efficiently in the case because their loss time is long. Figure 10 shows such a model, where $B = 100$ G and $n = 10^{11}$ cm^{-3}. The size of the LT and the injected particle temperatures remain the same as those in the previous model. Because the turbulence spectrum is flat ($q = 2$), we have a pretty hard accelerated proton distribution below 1 MeV. Above this energy, there is a cutoff due to the dominance of the escape term over the acceleration terms. The accelerated electron distribution has a cutoff at less than 100 keV, which is also due to the quick escape of electrons with higher energies from the acceleration site. At a few keV, both electron and proton distributions are quasi-thermal because of the dominance of Coulomb collisions.

The above results show that electrons can be accelerated to very high energies by parallel-propagating turbulent waves in pure hydrogen plasmas, but the presence of the acceleration barrier in the intermediate energy range makes the acceleration of protons very inefficient. Only in very weakly magnetized plasmas where the barrier is close to the background particle energy does the acceleration of protons become efficient. The required value of the plasma parameter α is above 10, which is much larger than that believed to be the case for solar flares. However, most astrophysical plasmas including solar flares are not made of pure hydrogen. They contain significant numbers of ^{4}He. These particles modify the dispersion relation used above. Abundances of elements heavier than He are too small to have a significant effect, but ^{4}He with an abundance (by number) of about 8% can have important effects.

To produce a near power-law distribution of the accelerated particles, the index of the turbulence spectrum must be larger
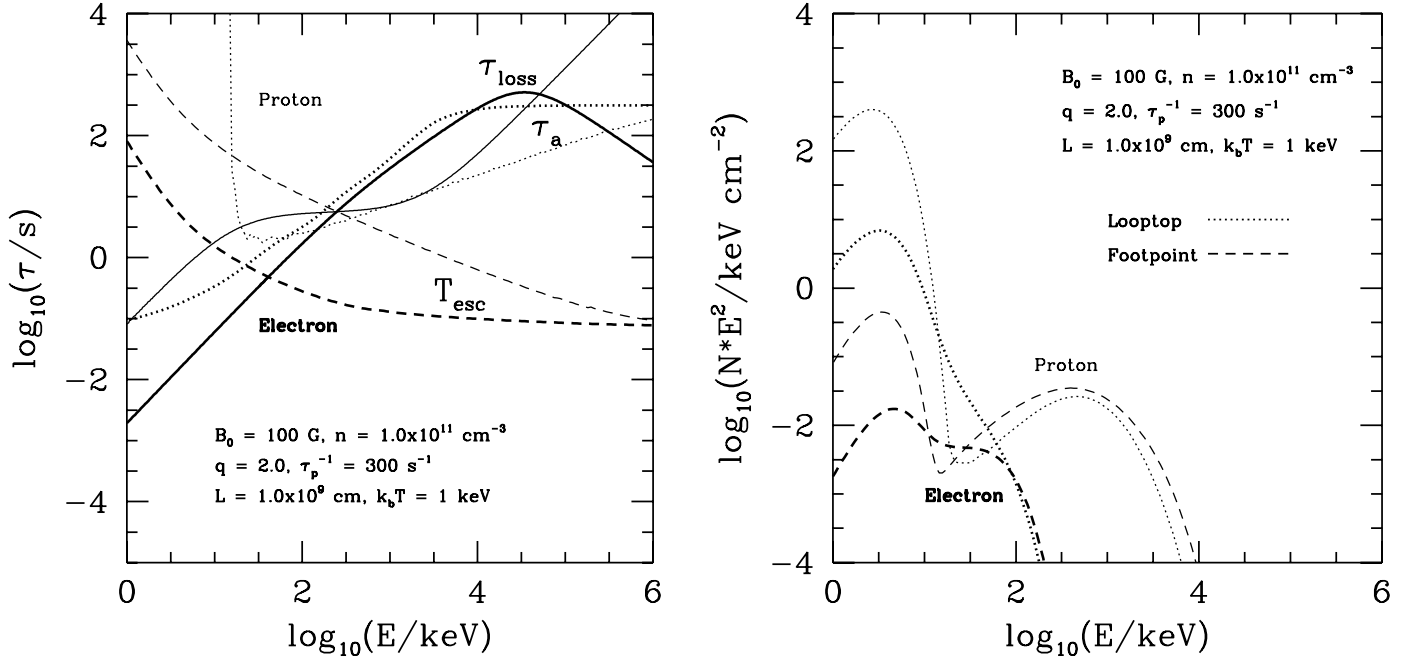
Fig. 10.—Same as Fig. 9, but for a model in a weakly magnetized plasma ($\alpha = 10$). The model parameters are shown in the figure. Here the proton acceleration becomes more efficient than the electron acceleration because its barrier is close to the energy of the injected particles and does not affect the acceleration processes. [*See the electronic edition of the Journal for a color version of this figure.*]

than 2 at high wavenumbers. If the turbulence is generated on a scale comparable to the size of the flaring loops, such a steep turbulence spectrum must flatten at low wavenumbers to ensure that the turbulence energy density is less than the energy density of the magnetic field, which is presumably the dominant source of energy for solar flares. Such a steepening of the turbulence spectrum at high k is expected if one includes the thermal damping effects of the waves with high wavenumbers. We incorporate these effects in the following discussion.

4. ACCELERATION IN HYDROGEN AND HELIUM PLASMAS

We now repeat the derivation of the previous section for more realistic plasmas containing electrons, protons, and α-particles. We assume a fully ionized H and ^{4}He plasma with the following relative abundances: electron/proton/ α-particle = 1/0.84/0.08.

4.1. *Dispersion Relation and Resonant Interactions*

The dispersion relation for such a plasma can be written as

$$\frac{k^2}{\omega^2} = 1 - \frac{\alpha^2}{\omega}\left[\frac{1}{\omega - 1} + \frac{(1 - 2Y_{He})\delta}{\omega + \delta} + \frac{Y_{He}\delta}{\omega + \delta/2}\right], \quad (28)$$

where the ^{4}He abundance $Y_{He} = 0.08$. The other symbols are the same as those defined in § 2.2.

The inclusion of ^{4}He splits the PC branch into two: one covers the frequency range of 0 to $-\delta/2$ and the other covers the frequency range of $-\omega_{PC}$ to $-\delta$, where $\omega_{PC} \simeq (0.5 + Y_{He})\delta$ is the lowest frequency of the branch (remember that the minus sign only indicates that the waves are left-handed polarized). We refer to the former as a ^{4}He cyclotron branch (HeC) and the latter as a modified proton-cyclotron branch

(PC$'$) because at high wavenumbers they approach the α-particle and proton-cyclotron frequencies, respectively. The left panels of Figure 11 show the dispersion relation in such a plasma and the resonance conditions for electrons and protons with $\beta = 0.5$ and $\mu = 0.12$.

With this additional branch, particles with $\mu \neq 0$ can interact at least with three waves with one from each of the three cyclotron branches (particles with $\mu = 0$ always interact with two waves from one of the wave branches). Some particles can resonate with five waves, three of which would be from one of the three cyclotron branches (e.g., the protons in the left panels of Fig. 11 have three resonances with the EC branch, with two of them shown in the bottom left panel; the third one is at high k and $w \to \Omega_e$). In a strongly magnetized plasma the two additional resonances can also come from the electromagnetic branches. The general results are quite similar to those in pure hydrogen plasmas; there are critical angles and critical energies, which now separate the μ-β and β-α spaces into regions with three and five resonant interactions. Given spectra for each of the wave branches, one can proceed to calculate the F-P coefficients, which have sharp jumps across the critical angles or energies and the times τ_{ac} and τ_{sc}. In the next section we discuss the turbulence spectrum we use for this purpose.

4.2. *Spectrum of Turbulence*

In the discussion of the previous section we assumed a power-law wave spectrum $\mathcal{E} \propto k^{-q}$, for $k > k_{min}$, with $k_{min} \ll k_A = \alpha\delta^{1/2}$ so that there will be waves with the Alfvénic dispersion relation for interactions with high-energy electrons and protons. We now introduce an additional cutoff at high wavenumbers presumably caused by thermal damping. Thus, we will have a broken power-law turbulence spectrum with three indexes q, q_l, and q_h and two critical wavenumbers k_{min} and k_{max}:
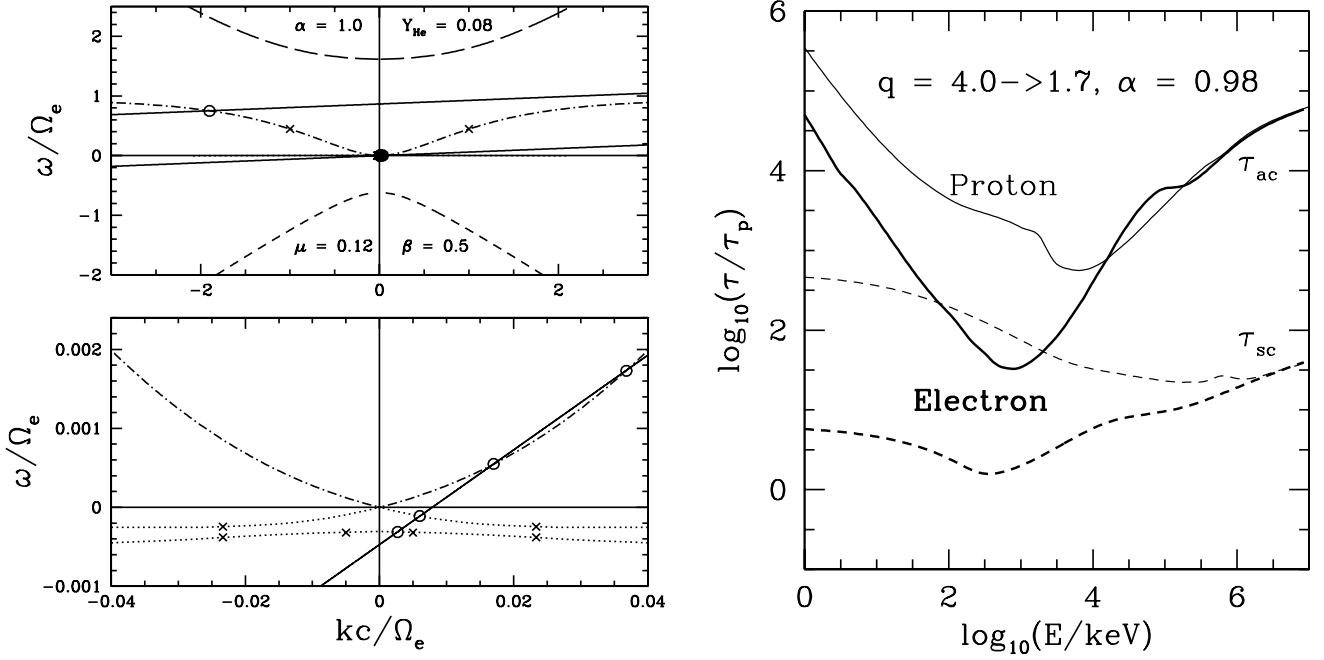
Fig. 11.—*Left* : Same as Fig. 1, but in an electron-proton-^{4}He plasma with $\alpha = 1.0$ and $Y_{\mathrm{He}} = 0.08$. The resonant interactions (*circles*) are for electrons (*upper line*) and protons (*lower line*) with $\beta = 0.5$ and $\mu = 0.12$. Here we note that there are two ion cyclotron branches (both indicated by the dotted lines); the upper one approaches the ^{4}He cyclotron waves at high k (HeC), while the lower one approaches the modified proton-cyclotron waves (PC′). The crosses indicate the expected breaks in the turbulence spectrum as discussed in the text. *Right* : Pitch-angle–averaged acceleration (*solid lines*) and scattering (*dashed lines*) times in units of τ_p for electrons (*thick lines*) and protons (*thin lines*). The model parameters are indicated in the figure. The minimum of the electron acceleration time corresponds to the spectral break k_{max} of the turbulence in the EC branch. See text for details. [*See the electronic edition of the Journal for a color version of this figure.*]

$$\mathcal{E}(k) = (q - 1)\frac{\mathcal{E}_0}{k_{\mathrm{min}}}$$

$$\times \begin{cases} \left(\dfrac{k}{k_{\mathrm{min}}}\right)^{q_l} & \text{for } k < k_{\mathrm{min}}, \\[2ex] \left(\dfrac{k}{k_{\mathrm{min}}}\right)^{-q} & \text{for } k_{\mathrm{min}} < k < k_{\mathrm{max}}, \\[2ex] \left(\dfrac{k_{\mathrm{max}}}{k_{\mathrm{min}}}\right)^{-q}\left(\dfrac{k}{k_{\mathrm{max}}}\right)^{-q_h} & \text{for } k > k_{\mathrm{max}}, \end{cases} \quad (29)$$

where $q_l > 0$ (we choose $q_l = 2$ because its value is almost irrelevant), $q = 1.7$ is the Kolmogorov value, and $q_h = 4$, a typical value of the spectral index for waves subject to strong damping (Vestuto et al. 2003). A self-consistent treatment of wave-particle interactions is required for an exact description of these spectral breaks. This is beyond the scope of the current investigation. Instead, we make some reasonable assumptions on these breaks:

1. The low k or large-scale cutoff $k_{\mathrm{min}} \gtrsim c/(\Omega_e L_{\mathrm{max}})$, where L_{max} is the largest scale of the turbulence, which must be less than the size L of the region and is most likely much less than it. To accelerate particles to high energies, we also need $k_{\mathrm{min}} \ll k_{\mathrm{A}} = \alpha/43$. For most waves we choose k_{min} as before, i.e., by the value of the highest energy we want the particles to achieve. However, such a choice for the PC′ branch results in a sharp feature in the spectrum of the accelerated protons. As can be seen in the bottom left panel of Figure 11, the PC′ branch, unlike the EC, PC, or HeC branches, crosses the frequency axis ($k = 0$) at a finite frequency $\omega_{\mathrm{PC}} \neq 0$. Such waves can resonantly scatter protons with a Lorentz factor of $\simeq 2/(1 + 2Y_{\mathrm{He}}) \sim 1.7$ or an energy of a few hundred MeV. If the spectrum of the PC′ branch wave extends to a very low wavenumber,

one would get very efficient acceleration at such energies and a sharp spectral feature. We assume that such a feature is not present (although there is no definite observation to rule it out) and cut off the spectrum of the PC′ waves at a higher $k_{\mathrm{min}} \simeq k_{\mathrm{A}}/5$ or a scale of $L_{\mathrm{max}} \simeq 400\pi c/\alpha\Omega_e$.

2. The high k or small-scale cutoff is determined via the damping of the waves by low-energy particles. For example, the cyclotron waves with high wavenumbers are subject to thermal damping in plasmas with a finite temperature (Schlickeiser & Achatz 1993; Steinacker et al. 1997; Pryadko & Petrosian 1998). One can introduce an imaginary ω to include this effect. The real part of ω is not very sensitive to the plasma temperature (Miller & Steinacker 1992). Hence, the cold plasma dispersion relation still gives a good description of the resonant interactions between waves and particles. However, above a wavenumber where the thermal damping time is comparable with the timescale of the wave cascade, the thermal damping steepens the spectrum of the turbulence. In the absence of a full treatment of these processes, we assume that the cyclotron waves have steeper spectra than the Whistler and Alfvén waves and set $k_{\mathrm{max}} = k_{\mathrm{W}} = \alpha$ for the EC branch. For the PC′ and HeC branches we set $k_{\mathrm{max}} = k_{\mathrm{A}} = \alpha\delta^{1/2}$. These spectral breaks are indicated by the crosses in the bottom left panel of Figure 11.

Recent studies of the transport of high-energy particles in the solar wind indicate that the resonance broadening due to the dissipation of turbulent plasma waves plays an essential role in explaining the observed long mean free paths of the particles (Bieber et al. 1994; Dröge 2003). Such broadening is also expected in our case. It will modify only equation (6) if the broadening width is less than the separation between the resonances. In the opposite (and unlikely) case the idea of resonant interaction is invalid. Because the resonance broadening mostly affects the scatterings of particles at relatively low
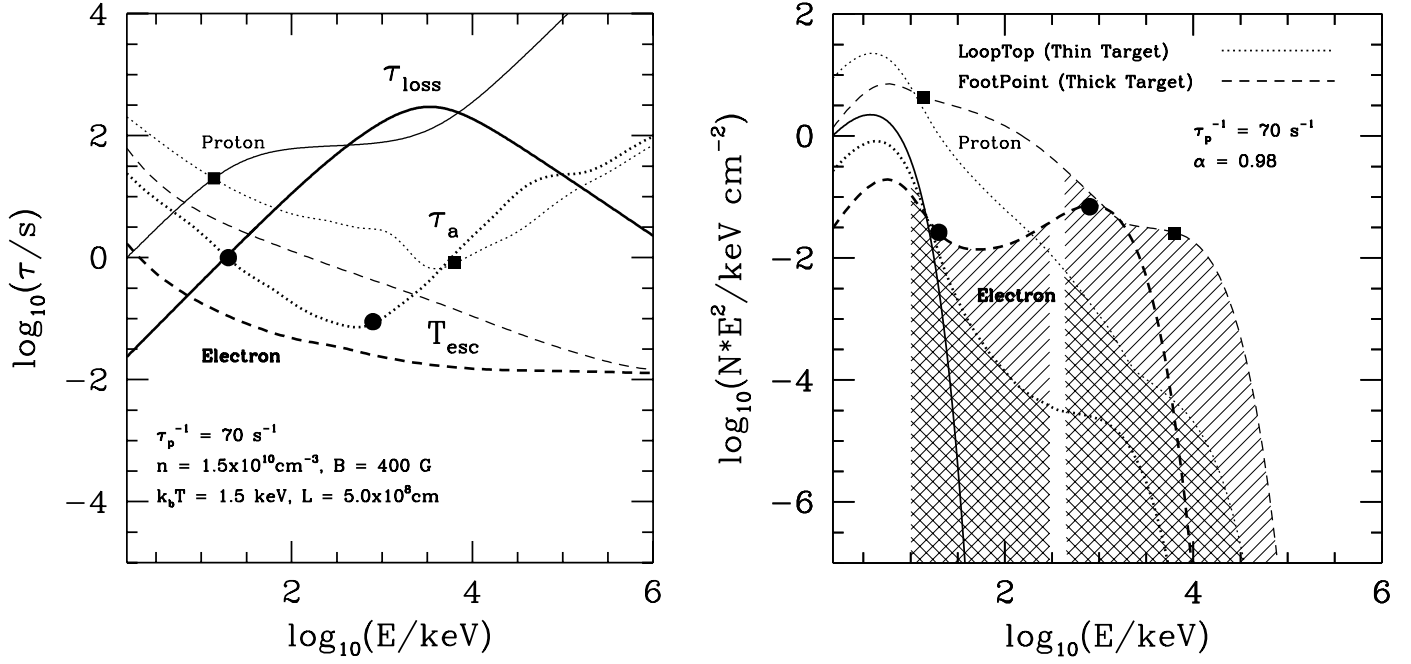
FIG. 12.—Same as Fig. 9, but for different model parameters (listed) and in a hydrogen and helium plasma. The energy content in high-energy electrons and protons is comparable. The hatched regions in the right panel correspond to the energy bands related to observations of the hard X-ray and gamma-ray emissions during the impulsive phase of solar flares. The signs indicate the spectral breaks of the accelerated particle distributions. [*See the electronic edition of the Journal for a color version of this figure.*]

energies, where Coulomb collisions are important under solar flare conditions, it is less important in understanding the particle acceleration processes studied here.

All the formulae developed in the previous sections are still valid except that now

$$\tau_p^{-1} = \frac{\pi}{2} \Omega_e \left(\frac{\mathcal{E}_0}{B_0^2/8\pi}\right)(q-1)k_{\min}^{q-1}, \qquad (30)$$

and the Alfvén velocity is given by $\beta_A = \delta^{1/2}/[\alpha(1 + 2Y_{He})^{1/2}]$. Because $q_l > 0$ and $q_h > q$ (and the PC′ branch contains much less energy than the other branches), the total turbulence energy density $\mathcal{E}_{tot} \simeq \mathcal{E}_0$.

The right panel of Figure 11 gives the electron (*thick lines*) and proton (*thin lines*) acceleration (*solid lines*) and scattering (*dashed lines*) times for a model with $\alpha = 1$. We see that in the high-energy range where particles are mostly interacting with the Alfvén waves, the times are almost the same as those in a pure hydrogen plasma. At low energies, the times rise sharply with the decrease of energy as a result of the thermal damping of the waves with high wavenumbers. As can be seen in the following discussion, the thermal damping makes the particle acceleration times match their escape times, giving near power-law accelerated particle distributions. More importantly, in the intermediate energy range, an acceleration barrier in the proton acceleration time still exists even though it is not as prominent as it is in a pure hydrogen plasma. This is mainly due to interactions with the HeC branch, which makes the acceleration of low-energy protons more efficient. The sharp decrease of the acceleration time with energy near the critical energy is still due to interaction with the Whistler waves. Comparing with Figure 8, we note that the electron acceleration and scattering times are also affected as evident by the wiggles seen at a few tens of MeV. These wiggles are due to interactions with the HeC and PC′ branches.

We emphasize here that $q = 1.7$ corresponds to the Kolmogorov spectrum. Our only assumption that may be ad hoc is the large-scale size cutoff for the PC′ branch waves. This assumption is not driven by observations but primarily introduced to obtain a smooth proton spectrum. We shall explore consequences of the assumption in the future. In the following discussion we fix these parameters at the specified values and investigate how the particle acceleration processes are affected by the strength of the turbulence $\mathcal{E}_{tot}$, the size of acceleration site L, the plasma parameter α, and the temperature of the injected particles. We show that this model gives much more reasonable explanations to solar flare observations than the previous one.

4.3. *Relative Acceleration of Electrons and Protons*

We now present some results on the relative numbers of accelerated electrons and protons at the acceleration site (LT) and escaping to the FPs. Here we explore its dependence on the model parameters. The normalization is as before (see Fig. 9 and discussion in eq. [21]), namely, we assume that the escape fluxes for the total numbers of electrons and protons are equal.

Figure 12 gives our fiducial model for solar flares where the energy content in the accelerated electrons and protons in the relevant observational energy bands (indicated by the shaded regions) is comparable. The timescales are given in the left panel, and the corresponding particle distributions are shown in the right panel. The line types are the same as those in Figure 9. The temperatures of the injected electrons and protons are $T = 1.5$ keV. The other model parameters are the size of the LT source $L = 5 \times 10^8$ cm, $n_e = 1.5 \times 10^{10}$ cm^{-3}, $B = 400$ G ($\alpha = 0.98$), and $\tau_p = 1/70$ s. These imply $8\pi\mathcal{E}_{tot}/B_0^2 \simeq 8.8 \times 10^{-9} k_{\min}^{-0.7}$, which is less than 10^{-3} for $k_{\min} > 2\pi c/L\Omega_e = 5.2 \times 10^{-8}$. Compared with models in pure hydrogen plasmas, the turbulence required to accelerate the
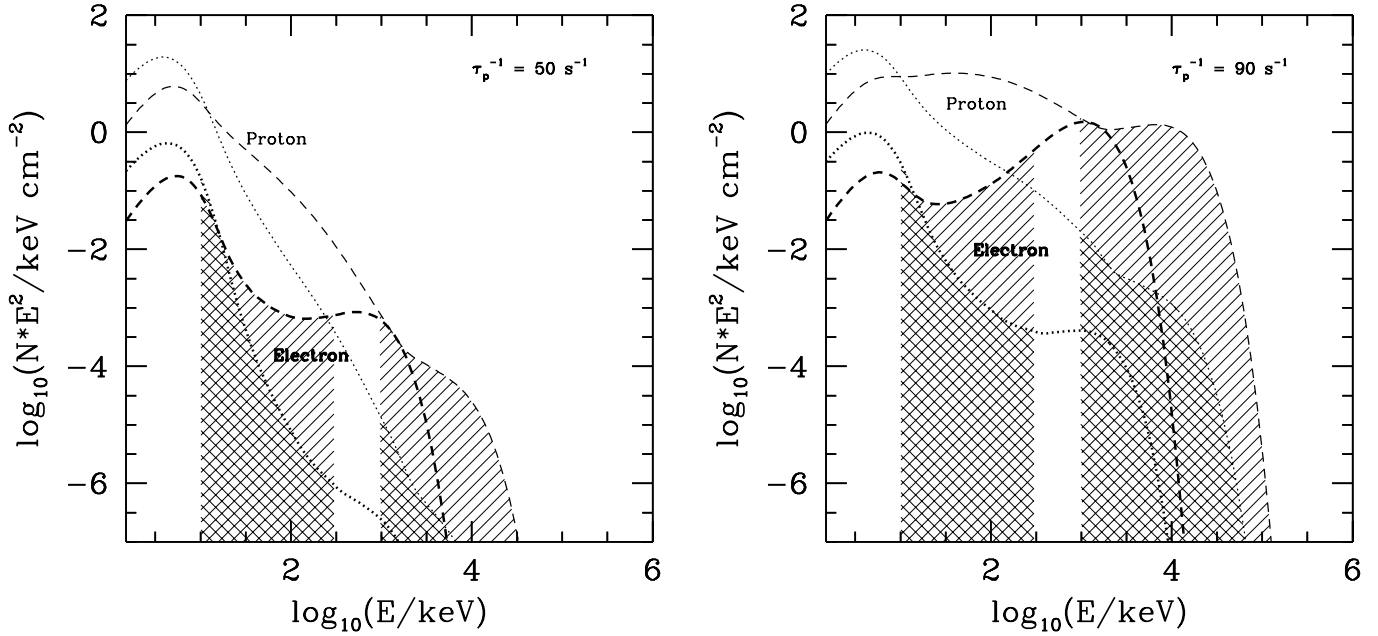
FIG. 13.—Same as the right panel of Fig. 12, but for two different values of τ_p, one larger (*left*) and one smaller (*right*). [*See the electronic edition of the Journal for a color version of this figure.*]

particles is much weaker in the current model. This is mainly because of the adopted Kolmogorov (instead of $q = 2$ or 3) turbulence spectrum at long wavelengths.

In Figure 13 we show the effects of the strength of turbulence on the particle acceleration. Because the acceleration time is proportional to τ_p but the escape time is inversely proportional to it, a small change in τ_p can make the acceleration and escape times off balance very quickly. The spectra of the accelerated particles then change dramatically with τ_p. However, because this is true for both electrons and protons, changes in the energy partition between electrons and protons are much smaller.

Another parameter that affects the spectra of the accelerated particles is the size L of the acceleration region. An increase of L results in an increase of the escape time and harder spectra of the accelerated particles. However, again because the escape times of electrons and protons increase by the same factor, the energy partition between them is not changed significantly. For example, for a model with $L = 10^9$ cm and $\tau_p^{-1} = 50$ s^{-1}, we find that the accelerated particle spectra are harder than those in the left panel of Figure 13 and more like those in the right panel of Figure 12.

Next we examine the effects of the plasma parameter $\alpha \propto n^{1/2}/B$. Figure 14 shows how the relative acceleration of electrons and protons changes with the change in the value of α. It turns out that for the range of parameters used in the current study, it does not matter whether α is changed by changing the value of the density n or the magnetic field B. The difference between these two possibilities will appear as relatively small changes in the spectra at the low- and high-energy ends where Coulomb collisions and synchrotron losses become important, respectively. To make the spectral shapes compatible with solar flare observations, the value of τ_p also needs adjustment. However, as we showed above, τ_p affects primarily the spectral hardness but not the relative acceleration of electrons and protons. Thus, the most relevant cause of the changes in the relative acceleration of protons and electrons is the variation of α; proton (and consequently other ions)

acceleration is more efficient in high-density and/or low magnetic field plasmas. Given that the acceleration of electrons and protons is dominated by different wave branches, it is not surprising that their relative acceleration depends on the plasma parameter α.

Finally, we consider the effects of the temperature of the background or injected particles. In the models discussed above, we use a high value of temperature of a few keV, which requires a preheating of the flaring plasma to a temperature above the quiet coronal value. *GOES* and *RHESSI* observations do suggest such a characteristic energy for the particles before the impulsive phase of X-ray flares. For example, *RHESSI*'s high-resolution spectra indicate that the electrons in the soft X-ray–emitting plasma always deviate from an isothermal distribution, implying a significant preheating of the flare plasma (Holman et al. 2003). The effects of the injection temperature are demonstrated in Figure 15, which shows particle spectra for models with temperatures different than that in the fiducial model (Fig. 12). All other model parameters remain the same. We see that the shapes of the spectra in the high-energy range do not change significantly. However, with the increase of the temperature, more particles reach the energy range where the acceleration rate is larger than the Coulomb collisional loss rate and are eventually accelerated to higher energies. At lower temperature, the quasi-thermal part of the spectra (similar to that of the injected particles) is more prominent, while at higher T the spectra of the accelerated particles are dominated by the nonthermal tails.

5. SUMMARY AND DISCUSSION

The primary aim of this work is the determination of the relative acceleration of electrons and protons by waves in a stochastic acceleration (SA) model. In this paper we present the results of the investigation of the resonant interaction of the particles with a broad spectrum of waves propagating parallel to the large-scale magnetic field. We calculate the acceleration and transport coefficients and determine the resulting spectra for both particles for physical conditions
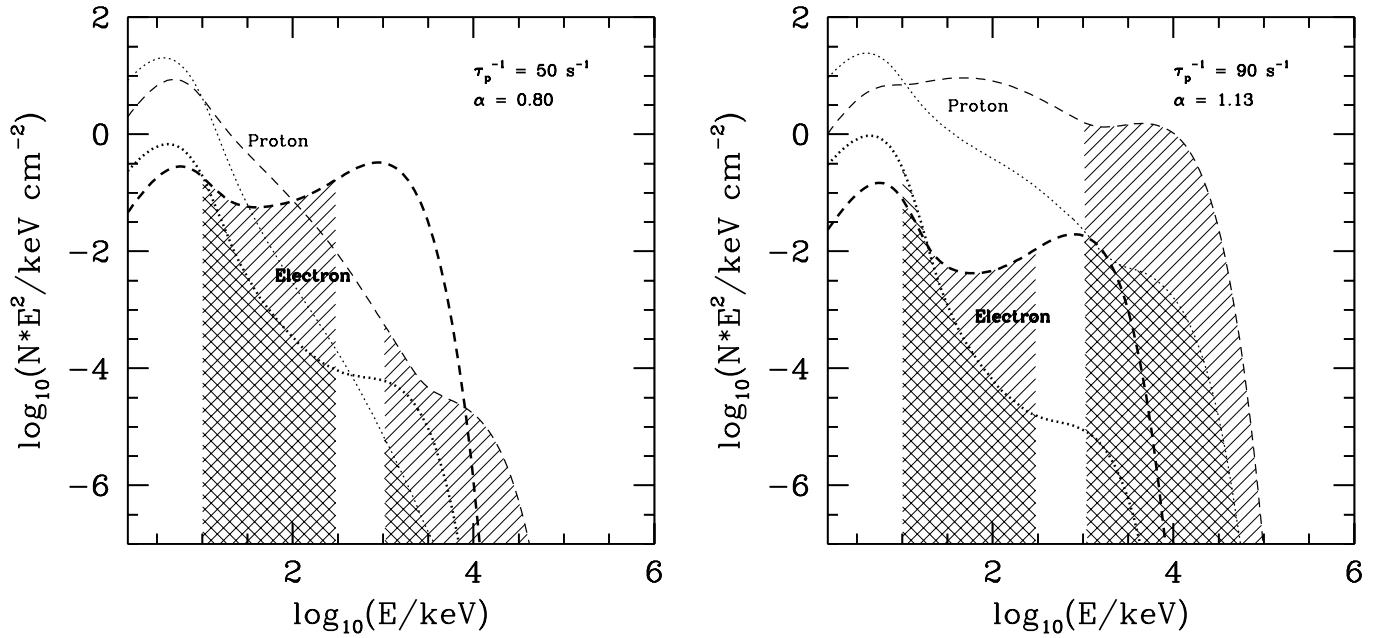
Fig. 14.—Same as Fig. 12, but for models with different plasma parameters α, which are indicated in the figures. The term τ_p is chosen such that the accelerated particle distributions are similar to that required to explain the impulsive hard X-ray emission from solar flares. The other model parameters are the same as those shown in Fig. 12. We see that the electron acceleration is favorable in strongly magnetized plasmas while the proton acceleration dominates in weakly magnetized plasmas. [*See the electronic edition of the Journal for a color version of this figure.*]

appropriate for solar flares. We show that the injection of such a turbulence in a magnetized hot plasma can accelerate both electrons and protons of the thermal background plasma to high energies in the acceleration site. Some of the accelerated particles escape the site and reach the FPs. The parameters that govern these processes are the density, temperature, magnetic field, size of the acceleration region, and the intensity and spectrum of the turbulence.

We first describe two general features of our results:

1. The first has to do with the general characteristics of the accelerated particle spectra. The outcome of the SA of a background thermal plasma is the presence of two distinct components. The first is a quasi-thermal component at low energies where Coulomb collisions play important roles. This can be considered as a simple heating process of the background
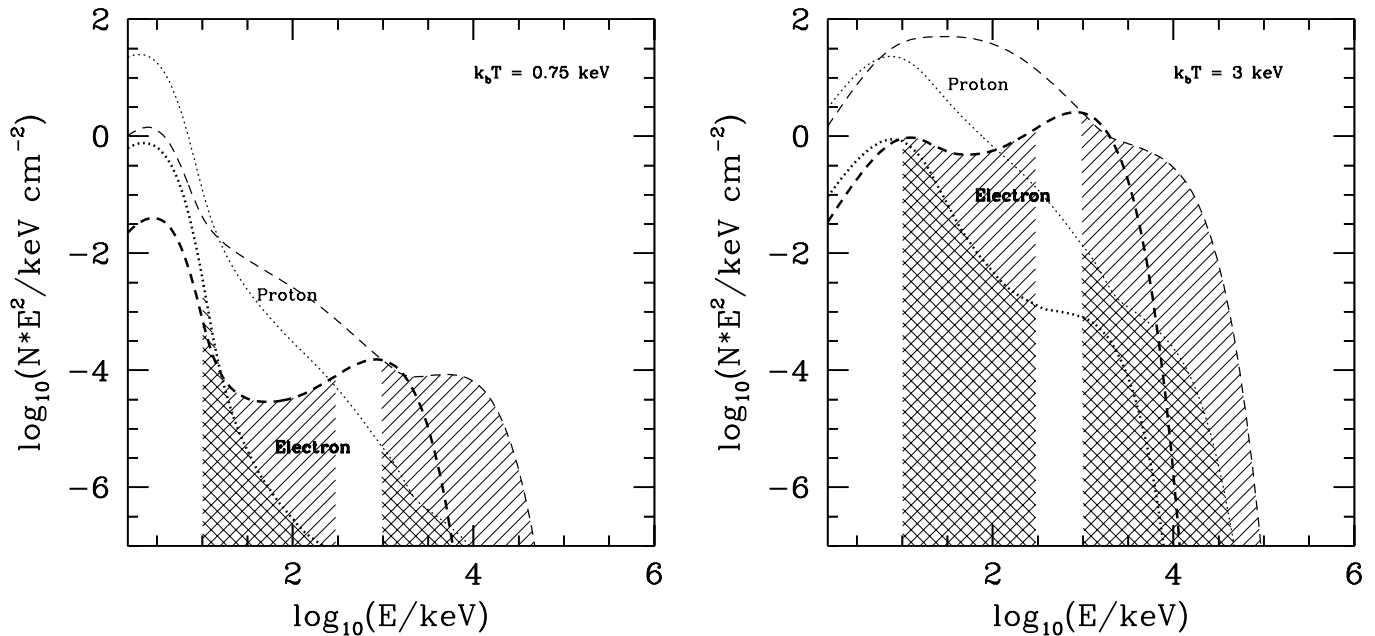

Fig. 15.—Same as Fig. 12, but for models with different temperatures for the injection plasma. The temperatures are indicated in the figures. Other model parameters remain the same as the fiducial model. The distributions of high-energy particles are not affected by the injection process. However, at low energies where Coulomb collisions dominate, many less particles are accelerated for an injection plasma with a lower temperature. [*See the electronic edition of the Journal for a color version of this figure.*]

plasma. The second is a nonthermal tail with a somewhat complex spectral shape. Technically, one can separate the two components at the energy where the Coulomb collisional loss rate $\dot{E}_{Coul}$ is equal to the direct acceleration rate A. We can then calculate the fractions of the turbulence energy that go to "heat" and to "acceleration." This explains the observation of both thermal and nonthermal emissions during the impulsive phase of solar flares.

The spectra of particles reaching the FPs are in general harder than the corresponding LT particle spectra because high-energy particles in the nonthermal tails escape more readily. The relative size of the two components in the acceleration site (LT) versus the FPs and for electrons versus protons depends sensitively on the model parameters, which can explain the large variation of the observed nonthermal emission among solar flares and other astrophysical sources.

2. The second feature has to do with the relative acceleration of electrons and protons. *To our knowledge, a new result of our investigation is that there is a significant difference in the acceleration of protons and electrons.* While the transport and acceleration coefficients for electrons are smooth functions of energy, this is not true for protons. There appears to be a barrier (lower rate) of acceleration for intermediate-energy protons. This can have a dramatic effect on the relative production rate and spectra of the accelerated protons and electrons.

To demonstrate some of this and other more subtle effects, we first investigated the acceleration of electrons and protons in pure hydrogen plasmas by turbulence with a simple power-law spectrum. We find that this simple model does not agree with some qualitative aspects of the observed accelerated particle distributions in solar flares. The barrier for protons is too strong for reasonable physical conditions. We then explore more realistic models, where we include the effects of the background ^{4}He particles and the thermal damping of the waves. These more realistic models are in better concordance with solar flare observations.

Specifically, we find the following:

1. In general, electrons are preferentially accelerated in more strongly magnetized plasmas (small $\alpha \propto n^{1/2}/B$), while the proton acceleration is efficient in more weakly magnetized plasmas. The ratio of the energy that goes into the accelerated electrons to that into protons is very sensitive to α, which can explain the wide range of the observed energy partition between these particles. The proton acceleration will be more efficient in larger loops where the magnetic field is presumably weaker and during the later phase of flares when the corona loops have been filled by plasmas evaporated from the chromosphere, giving a higher gas density. This can explain the offset of the centroid of the gamma-ray line emission (due to accelerated protons and ions) from that of the hard X-rays indicated by a recent *RHESSI* observation (Hurford et al. 2003). It can also account for the observed delay of the nuclear line emission relative to the hard X-ray emission (Chupp 1990).

2. The acceleration rates and spectra of both electrons and protons are very sensitive to the intensity of the turbulence and the size of the acceleration site. Models with more intense turbulence and/or larger acceleration region give rise to harder spectra. This result can explain the observed soft X-ray emission in advance of the impulsive phase hard X-ray and gamma-ray emissions (the so-called preheating) and the slower than expected decline of the temperature of the LT plasma in the gradual phase. When the turbulence is weak, as will be the case

at the beginning and end of a flare, almost all the dissipated turbulence energy goes into the quasi-thermal component and there is no significant hard component, producing soft X-ray emission without obvious hard X-ray or gamma-ray emission. When the strength of the turbulence exceeds a threshold, nonthermal tails and high-energy radiations ensue. On the other hand, for a turbulence energy much above this threshold, one would expect harder spectra than observed in solar flares. This may indicate that the sudden presence of a large amount of high-energy particles also introduces significant dissipation of the turbulence over a broad frequency range such that the strength of the turbulence is limited to a level close to the threshold. Consequently, we do not see flares with very flat X-ray spectra. To address these processes in detail, one needs to treat the wave generation, cascade, and damping by both low- and high-energy particles properly. Such an investigation is clearly warranted now but is beyond the scope of this paper.

3. In general, the spectra of both electrons and protons at the acceleration site (LT) are softer (stronger quasi-thermal component and steeper nonthermal spectrum) than the equivalent thick target spectra at the FPs. This is in excellent agreement with the results from the *Yohkoh* observations (Petrosian et al. 2002) and with the more convincing evidence from *RHESSI* observations (Jiang et al. 2003). The most important parameter here is the energy dependence of the escape time (see eq. [16]), which depends on the pitch-angle diffusion coefficient and the size of the acceleration region. Unlike the acceleration time (see item 2 in the first list of items in this section), the scattering and escape times for protons and electrons have similar general behaviors. Consequently, the difference between the LT and FP spectra is similar for both electrons and protons.

4. For injected plasmas with high temperatures, most of the particles can be accelerated to very high energies and the steady state particle distribution at low energies can be quite different from a thermal distribution. The presence of a quasi-thermal component is typical for low-temperature plasmas.

5. There are high-energy cutoffs (at around 1 MeV for electrons and 10 MeV for protons) in the accelerated particle spectra. Both cutoffs are due to the quick escape and the relatively inefficient acceleration of higher energy particles. The locations of these cutoffs are directly related to the higher wavenumber spectral breaks in the turbulence spectrum. In plasmas with stronger thermal damping, the acceleration of high-energy particles becomes relatively more efficient than that of low-energy particles. Consequently, the cutoffs shift toward higher energies. We would then expect a positive correlation between the cutoff energies and the heating rate of the background plasma. Observations over a broad energy range will be able to test this prediction.

Finally, we summarize several improvements that are required for direct comparisons with observations:

1. The results presented here show that wave-particle interactions play crucial roles in solar flares, especially during the impulsive phase. A self-consistent treatment of this problem requires the solution of the coupled kinetic equations for both particles and waves. Previous studies on this aspect focused on the Alfvén waves alone and ignored the energy-dependent escaping processes (Miller & Roberts 1995; Miller et al. 1996). Incorporation of the current investigation will make the models more realistic.

Waves propagating obliquely with respect to the large-scale magnetic field will introduce new features to the wave-particle

interaction (Pryadko & Petrosian 1999). Earlier studies have shown that the fast-mode waves are very efficient in heating or accelerating super-Alfvénic particles via Landau damping or transit-time damping (Miller et al. 1996; Quataert 1998; Schlickeiser & Miller 1998). These waves are expected to enhance the acceleration of high-energy electrons and protons, and sub-Alfvénic particles may also be accelerated when one adopts the exact dispersion relation for the waves. Results similar to what we present here are expected. Moreover, if the turbulence is dominated by the lower hybrid waves, electrons will not be scattered efficiently so that the electron distribution is not isotropic (Luo et al. 2003). The acceleration barrier may not exist if this is also true for protons. A comprehensive study including these waves is needed to address the heating and acceleration processes more completely.

2. A time-dependent model is needed to address the temporal characteristics of solar flares and the injection processes. Here we assume that the system is in a steady state and the injection fluxes of protons and electrons are equal. This may be the case if the plasmas are brought into the acceleration site by the reconnecting magnetic fields. However, e.g., if electrons have a shorter escape time than protons, there could be a net charge flux from the acceleration site, which would induce reverse currents consisting mainly of electrons so that the injection fluxes of electrons and protons into the acceleration site will be different.

3. The application of the formalism developed here to the acceleration of other ions is straightforward. We are in the process of evaluating the relative acceleration of different ion species and isotopes, and the results are promising and will be published in future papers. It is also straightforward to apply the formalism to accretion systems of black holes and neutron stars. Besides the magnetic reconnection, turbulent plasma waves can also be produced by the magnetorotational instability in accretion disks (Balbus & Hawley 1991).

APPENDIX A

DISPERSION RELATIONS FOR THE EC AND PC BRANCHES

Waves in the EM$'$ branch interact resonantly with protons, and those in the EM branch interact with electrons only for low values of α. These interactions mostly affect the acceleration of very low energy particles (see discussion in § 3.2). Waves in the EC and PC branches are the dominant modes for the acceleration of protons and electrons for intermediate and high values of α and energies and therefore play key roles in determining the relative acceleration of the two species. In what follows we give some approximate analytic descriptions of these modes that are considerably simpler than equation (22).

At frequencies $\omega \ll \delta$, or $|k| \ll k_A \equiv \alpha \delta^{1/2}$, both branches reduce to the Alfvén waves with the dispersion relation $\omega = |k|\beta_A = \delta(|k|/k_A)$ for the EC branch. The middle portion of the EC branch, $k_A \ll |k| \ll k_W \equiv \alpha$, corresponds to the Whistler waves with the dispersion relation $\omega \simeq k^2/\alpha^2 = (k/k_W)^2$. At still higher wavenumbers ($|k| \gg k_W$), $\omega \to 1$ and the dispersion relation can be approximated as $\omega \sim 1 - \alpha^2/k^2$. The transition between the Whistler and this portion occurs at $k_W = \alpha$. This suggests that the dispersion relation for the Whistler and electron-cyclotron portions can be approximately described by $\omega = k^2/(k^2 + \alpha^2)$. For the EC branch we can use the simple approximation

$$\omega = \frac{\delta^{1/2}x + x^2}{1 + x^2}, \qquad x = |k|/k_W = |k|/\alpha, \tag{A1}$$

which agrees with the exact expression within 40% for $\alpha \geq 0.6$. For highly magnetized plasmas with $\alpha \ll 1$ the Whistler branch disappears. One then has $\omega = |k|$ for $|k| < 1$ and $\omega = 1$ for $|k| > 1$ for the EC branch (and the reverse is true for the EM branch).

Similarly for the PC branch, one gets the Alfvén waves with $\omega = -|k|\beta_A$ at low wavenumbers ($|k| \ll k_A$). The proton-cyclotron waves whose dispersion relation does not have a simple form can be roughly approximated as $\omega_{PC} \sim -\delta\{1 - 1/[2 + (k/k_A)^2]\}$ for high k. We can combine these two forms into one simple expression,

$$\omega = -\delta \frac{y + y^2}{1 + y + y^2}, \qquad y = |k|/k_A = |k|/\left(\alpha \delta^{1/2}\right), \tag{A2}$$

which agrees with the exact expression to within 10% for $\alpha \geq 0.6$. For very highly magnetized plasmas, $\alpha \ll \delta^{1/2}$, one again has $\omega = -|k|$ for $|k| < \delta$ and $\omega = -\delta$ for $|k| > \delta$ for the PC branch (and the reverse for the EM$'$ branch).

APPENDIX B

CRITICAL ENERGIES AND ANGLES FOR RESONANCE WITH THE EC AND PC BRANCHES

With the approximate analytical expressions (A1) and (A2) for the dispersion relation, one can derive the critical velocity (eq. [24]) and critical angle (eq. [25]) for resonant interactions of low-energy particles with the EC and PC branches. The critical velocity is for protons with $\mu = 1$ interacting with the EC branch. From the resonance condition given by equation (4) and the dispersion relation given by equation (A1) for the EC branch, we have

$$\alpha\beta x - \frac{\delta}{\gamma} = \frac{\delta^{1/2}|x| + x^2}{1 + x^2}, \qquad x = k/k_W = k/\alpha. \tag{B1}$$

This equation has three roots, with two of them being equal and $\ll 1$ at the critical velocities (see Fig. 1 and eq. [24]). We can therefore ignore the x^2 term in the denominator of the right-hand side of equation (B1). One can show that

$$\beta_{cr} = 3\sqrt{\delta}/\alpha \simeq 0.07/\alpha, \tag{B2}$$

which agrees with the numerical result within 15% (eq. [24]). In general, we have

$$\beta_{cr} = 3\sqrt{\delta}/\mu\alpha \simeq 0.07/\mu\alpha. \tag{B3}$$

For electron resonances with the EC branch, we have

$$\alpha\beta\mu x + \frac{1}{\gamma} = \frac{\delta^{1/2}|x| + x^2}{1 + x^2}. \tag{B4}$$

The equation has three roots, with two of them being equal when

$$(\alpha\beta\gamma\mu_{cr})^2 = \frac{8(\gamma - 1)^3}{8 + 20\gamma - \gamma^2 + \sqrt{(8 + 20\gamma - \gamma^2)^2 + 64(\gamma - 1)^3}}. \tag{B5}$$

We then have

$$\mu_{cr} \simeq \beta^2/\sqrt{54}\alpha \qquad \text{for } \beta \ll 1, \tag{B6}$$

which agrees with equation (25) within 5%.
   For proton resonance with the PC branch, we have

$$\alpha\beta\mu\sqrt{\delta}y - \frac{\delta}{\gamma} = -\delta\frac{|y| + y^2}{1 + |y| + y^2}, \qquad y = k/\sqrt{\delta}\alpha. \tag{B7}$$

For low-energy protons at critical pitch angles, the two equal roots of the equation are much larger than unity. We can therefore approximate the right-hand side of this equation as $-\delta(1 - 1/y^2)$. Then we have

$$\frac{4}{27}\frac{\delta}{(\alpha\beta\gamma\mu_{cr})^2} = \left(\frac{\gamma}{\gamma - 1}\right)^3, \tag{B8}$$

which becomes

$$\mu_{cr} = \sqrt{\delta}\beta^2/\sqrt{54}\alpha \qquad \text{for } \beta \ll 1. \tag{B9}$$

This agrees with equation (25) within 5%.

APPENDIX C

APPROXIMATE ANALYTIC EXPRESSIONS FOR THE ACCELERATION AND SCATTERING TIMES IN THE RELATIVISTIC AND LOW-ENERGY LIMITS

It is useful to have some approximate analytical expressions for the acceleration and scattering times under certain limits. In the relativistic region where $\gamma \gg 1$, the results for electrons are relatively simple and have been studied under different contexts (Schlickeiser 1989; PP97). Here we discuss the results for ions. For relativistic particles, and in general for weakly magnetized plasmas ($\alpha > \delta^{1/2}$), $R_1 \gg R_2^2$. As a result, the acceleration time defined by equation (12) can be approximated as

$$\tau_{ac}^{-1} = \langle D_{pp}/p^2 \rangle, \tag{C1}$$

where angle brackets denote the average over pitch angle. Relativistic particles with $\gamma \gg |\omega_i|/\delta$ resonate with the Alfvén waves with $\omega = \pm\beta_A k$. From the resonance condition given by equation (4), we have the wavenumbers of the resonant waves: $k_{\pm} = \omega_i/[\gamma(\beta\mu \mp \beta_A)] \simeq \omega_i\beta\mu/\gamma$. Then we have

$$\left\langle \frac{D_{pp}\tau_{pi}}{p^2} \right\rangle = \frac{\gamma^{q-2}\beta_{\mathrm{A}}^2}{|\omega_i|^q \beta^2} \int_0^1 d\mu \left(1 - \mu^2\right) \left[(|\beta\mu - \beta_{\mathrm{A}}|)^{q-1} + (|\beta\mu + \beta_{\mathrm{A}}|)^{q-1} \right]$$

$$\approx \frac{\gamma^{q-2}\beta_{\mathrm{A}}^2}{|\omega_i|^q \beta^2} \int_0^1 d\mu \left(1 - \mu^2\right) 2(\beta\mu)^{q-1} = \frac{4\gamma^{q-2}\beta^{q-3}\delta}{q(q+2)\alpha^2 |\omega_i|^q}, \tag{C2}$$

which is consistent with the numerical results within a factor of 2.

Similarly, one can estimate the scattering time in the relativistic limit:

$$\frac{\tau_{\mathrm{sc}}}{\tau_{pi}} = 2|\omega_i|^q \gamma^{2-q} \left\langle \frac{(1 - \mu^2)}{(\beta\mu - \beta_{\mathrm{A}})^{q-1} + (\beta\mu + \beta_{\mathrm{A}})^{q-1}} \right\rangle$$

$$\approx \frac{|\omega_i|^q}{\gamma^{q-2}\beta^{q-1}} \left[\frac{1 - (\beta_{\mathrm{A}}/\beta)^{2-q}}{2-q} - \frac{1 - (\beta_{\mathrm{A}}/\beta)^{4-q}}{4-q} \right], \tag{C3}$$

which is in agreement with the numerical results within 50%. Note that the integral over μ has been taken from β_{A}/β to 1 here. Like the acceleration time, protons and electrons with the same energy have the same scattering time. This is consistent with the result of PP97. We note that in the relativistic region the acceleration and scattering times are identical for all charged particles except for the ω_i term.

In the nonrelativistic region where $\gamma \approx 1$, from the resonance condition $\omega = -\omega_i + \beta\mu k$ and the dispersion relation given by equation (22), one can show that

$$k = -\omega\alpha (\beta\mu k)^{-1/2}. \tag{C4}$$

Thus, $k = (\omega_i^2 \alpha^2 \beta^{-1} \mu^{-1})^{1/3}$. Using equation (5), we have

$$\left\langle \frac{D_{pp}\tau_{pi}}{p^2} \right\rangle \approx \left\langle \frac{1 - \mu^2}{3\alpha^2\beta^2} \left(\frac{|\omega_i|^2 \alpha^2}{\beta\mu} \right)^{(1-q)/3} \right\rangle$$

$$= \frac{6}{(q+2)(q+8)} \left(\alpha^{-2(q+2)} |\omega_i|^{2(1-q)} \beta^{q-7} \right)^{1/3}. \tag{C5}$$

We note that $\beta_g \approx -2\beta\mu$ under the resonance condition. In a previous study (PP97), the minus sign was missed, which causes their acceleration time to be 3 times shorter than ours. Equation (5) then gives

$$\langle D_{\mu\mu}\tau_{pp} \rangle \approx \left\langle \left[1 + \frac{\mu(|\omega_i|\alpha\beta\mu)^{1/3}}{\beta\alpha} \right]^2 \frac{1 - \mu^2}{3\beta\mu} \left(\frac{\omega_i^2 \alpha^2}{\beta\mu} \right)^{-q/3} \right\rangle$$

$$\approx 6\beta^{q/3-1} (|\omega_i|\alpha)^{-2q/3} \left[\frac{1}{q(q+6)} + \frac{2|\omega_i|^{1/3}}{(q+4)(q+10)(\alpha\beta)^{2/3}} + \frac{|\omega_i|^{2/3}}{(q+8)(q+14)(\alpha\beta)^{4/3}} \right], \tag{C6}$$

which agrees with the numerical results within 20%.

APPENDIX D

APPROXIMATE ANALYTIC EXPRESSION FOR THE ACCELERATION BARRIER

To estimate the acceleration time at the barrier in pure hydrogen plasmas, we notice that resonant interactions of protons with nearly 90° pitch angle ($\mu < \mu_{\mathrm{cr}}$) with proton-cyclotron waves moving in both directions have significant contributions to the proton acceleration below the critical energy. Because $D_{\mu\mu}(R_1 - R_2^2)$ is a smooth function near $\mu = 0$ (Fig. 5) and $\mu_{\mathrm{cr}} \ll 1$ (eq. [25]), we have

$$\tau_{\mathrm{ac}}(p) \approx \frac{p^2}{D_{pp}(\mu = 0, \, p)\mu_{\mathrm{cr}}(p)}. \tag{D1}$$

Beyond the critical energy, some protons start to resonate with Whistler waves (see Fig. 2) and the proton acceleration rate increases sharply with energy.

From equation (5), we have

$$\frac{D_{pp}(\mu = 0, \, p)}{p^2} = \frac{2\beta_{ph}^2 |k|^{-q}}{\tau_{pp}\gamma^2\beta^2 |\beta_g|}, \tag{D2}$$

where k can be obtained from the dispersion relation given by equation (22) and $\omega = -\delta/\gamma$ is given by the resonance condition given by equation (4). Then we have

$$
\begin{aligned}
\tau_{\mathrm{ac}} &\approx \frac{\tau_p \gamma^{2-q} \beta^2 \delta^{q-2}}{2\mu_{\mathrm{cr}}} \left[1 + \frac{\alpha^2 \gamma^2 (1+\delta)}{\delta(\delta+\gamma)(\gamma-1)} \right]^{(3+q)/2} \left\{ 1 + \frac{\alpha^2 (1+\delta)[\gamma - 0.5(1-\delta)]\gamma^3}{(\delta+\gamma)^2 (\gamma-1)^2 \delta} \right\}^{-1} \\
&\approx \frac{2^{(q-1)/2} \tau_p \delta^{(q-5)/2} \alpha^{q+1}}{\mu_{\mathrm{cr}}} \beta^{3-q} \qquad \text{for } \beta \ll 1 \\
&= 7\alpha^{q+2} (2\delta)^{(q-1)/2} \beta^{1-q} \delta^{-5/2} \tau_p \\
&= 7\alpha^{q+2} \delta^{-5/2} \left(\frac{E}{m_e c^2} \right)^{(1-q)/2} \tau_p.
\end{aligned}
\tag{D3}
$$

Combining this with equations (B2) and (C2), one can estimate the height of the acceleration barrier in logarithmic scale at the critical velocity

$$
\delta \log(\tau_{\mathrm{ac}}) \simeq \log\left\{ (3.1) 2^{(q-1)/2} \alpha^{q+2} \delta^{-1/2-q} / [q(q+2)] \right\}.
\tag{D4}
$$

Similarly, one can estimate the acceleration time for low-energy electrons:

$$
\begin{aligned}
\tau_{\mathrm{ac}} &= 2 \left[\int_{-1}^{1} d\mu \, D_{\mu\mu} \left(R_1 - R_2^2 \right) \tau_p \right]^{-1} \\
&\approx \frac{\tau_p \gamma^{2-q} \beta^2}{2\mu_{\mathrm{cr}}} \left[1 + \frac{\alpha^2 \gamma^2 (1+\delta)}{(\gamma-1)(1+\gamma\delta)} \right]^{(3+q)/2} \left\{ 1 + \frac{\alpha^2 (1+\delta)[\gamma\delta + 0.5(1-\delta)]\gamma^3}{(\gamma-1)^2 (1+\gamma\delta)^2} \right\}^{-1} \\
&= 7\alpha^{q+2} \left(\frac{E}{m_e c^2} \right)^{(1-q)/2} \tau_p \qquad \text{for } \beta \ll 1.
\end{aligned}
$$

These expressions are consistent with the numerical results within a factor of 2. The discrepancy is large for turbulence with a flat spectrum. This is mainly due to contributions from electron-cyclotron and proton-cyclotron waves to the acceleration of particles with two resonances. When the turbulence spectrum becomes flatter, their contributions to the pitch-angle–averaged acceleration time become more important. However, as we discussed in § 4, this effect is not important in the real astrophysical situation where the cyclotron waves are damped. Thus, the analytical expressions give a good estimate of acceleration time in the intermediate energy range.

REFERENCES

Balbus, S. A., & Hawley, J. F. 1991, ApJ, 376, 214
Barbosa, D. D. 1979, ApJ, 233, 383
Bech, F. W., Steinacker, J., & Schlickeiser, R. 1990, Sol. Phys., 129, 195
Bieber, J. W., et al. 1994, ApJ, 420, 294
Chupp, E. L. 1990, Science, 250, 229
Dröge, W. 2003, ApJ, 589, 1027
Dung, R., & Petrosian, V. 1994, ApJ, 421, 550 (DP94)
Ginzburg, V. L., & Syrovatskii, S. I. 1964, The Origin of Cosmic Rays (New York: Pergamon)
Hamilton, R. J., & Petrosian, V. 1992, ApJ, 398, 350
Holman, G., Sui, L., Schwartz, R., & Emslie, G. 2003, ApJ, 595, L97
Hua, X. M., & Lingenfelter, R. E. 1987a, ApJ, 323, 779
———. 1987b, Sol. Phys., 107, 351
Hua, X. M., Ramaty, R., & Lingenfelter, R. E. 1989, ApJ, 341, 516
Hurford, G. J., Schwartz, R. A., Krucker, S., Lin, R. P., Smith, D. M., & Vilmer, N, 2003, ApJ, 595, L77
Jiang, Y. W., Liu, W., Petrosian, V., & McTiernan, J. 2003, AAS, 34, 18.03
Kennel, C. F., & Engelmann, F. 1966, Phys. Fluids, 9, 2377
Kirk, J. G., Schneider, P., & Schlickeiser, R. 1988, ApJ, 328, 269
Kozlovsky, B., Murphy, R. J., & Ramaty, R. 2002, ApJS, 141, 523
Leach, J. 1984, Ph.D. thesis, Stanford Univ.
Liu, W., Jiang, Y. W., Petrosian, V., & Metcalf, T. R. 2003, AAS, 34, 18.02
Luo, Q. Y., Wei, F. S., & Feng, X. S. 2003, ApJ, 584, 497
Masuda, S. 1994, Ph.D. thesis, Univ. Tokyo
Masuda, S., Kosugi, T., Hara, H., Tsuneta, S., & Ogawara, Y. 1994, Nature, 371, 495
Mazur, J. E. Mason, G. M., Klecker, B., & McGuire, R. E. 1992, ApJ, 401, 398
Miller, J. A. 2003, in Multi-Wavelength Observations of Coronal Structure and Dynamics, ed. C. H. Petrus et al. (COSPAR Colloq. Ser. 13; New York: Pergamon), 387
Miller, J. A., LaRosa, T. N., & Moore, R. L. 1996, ApJ, 461, 445
Miller, J. A., & Ramaty, R. 1987, Sol. Phys., 113, 195

Miller, J. A., & Roberts, D. A. 1995, ApJ, 452, 912
Miller, J. A., & Steinacker, J. 1992, ApJ, 399, 284
Miller, J. A., et al. 1997, J. Geophys. Res., 102, 14631
Park, B. T., & Petrosian, V. 1995, ApJ, 446, 699
———. 1996, ApJS, 103, 255
Park, B. T., Petrosian, V., & Schwartz, R. A. 1997, ApJ, 489, 358
Petrosian, V., & Donaghy, T. Q. 1999, ApJ, 527, 945
Petrosian, V., Donaghy, T. Q., & McTiernan, J. M. 2002, ApJ, 569, 459
Petrosian, V., McTiernan, J. M., & Marschhäuser, H. 1994, ApJ, 434, 747
Post, E. F. 1956, Rev. Mod. Phys., 28, 338
Pryadko, J. M., & Petrosian, V. 1997, ApJ, 482, 774 (PP97)
———. 1998, ApJ, 495, 377
———. 1999, ApJ, 515, 873
Quataert, E. 1998, ApJ, 500, 978
Ramaty, R. 1979, in AIP Conf. Proc. 56, Particle Acceleration Mechanisms in Astrophysics, ed. J. Arons, C. Max, & C. McKee (New York: AIP), 135
Ramaty, R., Kozlovsky, B., & Lingenfelter, R. E. 1975, Space Sci. Rev., 18, 341
———. 1979, ApJS, 40, 487
Reames, D. V., Meyer, J. P., & von Rosenvinge, T. T. 1994, ApJS, 90, 649
Rieger, E., Gan, W. Q., & Marschhäuser, H. 1998, Sol. Phys., 183, 123
Schlickeiser, R. 1989, ApJ, 336, 243
———. 2002, Cosmic Ray Astrophysics (Berlin: Springer)
Schlickeiser, R., & Achatz, U. 1993, J. Plasma Phys., 49, 63
Schlickeiser, R., & Miller, J. A. 1998, ApJ, 492, 352
Spitzer, L. 1956, Physics of Fully Ionized Gases (New York: Wiley)
Steinacker, J., Meyer, J. P., Steinacker, A., & Reames, D. V. 1997, ApJ, 476, 403
Steinacker, J., & Miller, J. A. 1992, ApJ, 393, 764
Sturrock, P. 1994, Plasma Physics (Cambridge: Cambridge Univ. Press)
Vestuto, J., Ostriker, E., & Stone, J. M. 2003, ApJ, 590, 858